A novel method for comparison of arterial remodeling in hypertension: quantification of arterial trees and recognition of remodeling patterns on histological sections

Alex A. Gutsol[1*], Paula Blanco[2], Svetlana I. Samokhina[3], Sergey A. Afanasiev[4], Chris R.J. Kennedy[1], Sergey V. Popov[4], Kevin D. Burns[5]

[1]Kidney Research Centre, Ottawa Hospital Research Institute, University of Ottawa, ON, Canada

[2]Department of Pathology and Laboratory Medicine, University of Ottawa, ON, Canada

[3]Tomsk State University, Tomsk, Russian Federation

[4]Cardiology Research Institute, Tomsk, Russian Federation

[5]Division of Nephrology, Department of Medicine, University of Ottawa, ON, Canada

E-mail: agutsol@uottawa.ca (AG)

Abstract

Remodeling of spatially heterogeneous arterial trees is routinely quantified on tissue sections by averaging linear dimensions, with lack of comparison between different organs and models. The impact of experimental models or hypertension treatment modalities on organ-specific vascular remodeling remains undefined. A wide variety of arterial remodeling types has been demonstrated for hypertensive models, which include differences across organs. The purpose of this study was to reassess methods for measurement of arterial remodeling and to establish a

morphometric algorithm for standard and comparable quantification of vascular remodeling in hypertension in different vascular beds. We performed a novel and comprehensive morphometric analysis of terminal arteries in the brain, heart, lung, liver, kidney, spleen, stomach, intestine, skin, skeletal muscle, and adrenal glands of control and Goldblatt hypertensive rats on routinely processed tissue sections. Mean dimensions were highly variable but grouping them into sequential 5 μm intervals permitted creation of reliable linear regression equations and complex profiles. Averaged arterial dimensions demonstrated seven remodeling patterns that were distinct from conventional inward-outward and hypertrophic-eutrophic definitions. Numerical modeling predicted at least twenty variants of arterial spatial conformations. Recognition of remodeling variants was not possible using averaged dimensions, their ratios, or the remodeling and growth index. To distinguish remodeling patterns, a three-dimensional modeling was established and tested. The proposed algorithm permits quantitative analysis of arterial remodeling in different organs and may be applicable for comparative studies between animal hypertensive models and in human hypertension. Arterial wall tapering is the most important factor to consider in arterial morphometry, while perfusion fixation with vessel relaxation is not necessary. Terminal arteries in organs undergo the same remodeling pattern in Goldblatt rats, except for organs with hemodynamics affected by the arterial clip. The existing remodeling nomenclature should be replaced by a numerical classification applicable to any type of arterial remodeling.

Author summary

Arterial hypertension effects modern nations and is characterised by systemic hypertensive angiopathy that affects all organs. Arterial remodeling is a main factor to be analyzed in animal models and human. Despite abundant data, there is a significant lack of comparative analysis on

arterial remodeling. The data from the present study have established a novel methodological approach to assess and compare arterial remodeling in hypertension. We have developed an effective algorithm for morphometry of intra-organ arteries to standardize remodeling assessment and allow comparisons between different hypertensive models, organs and species. Our study opens the possibility to assess remodeling using conventional widely used histological tissue sections with no need for special perfusion-fixation. The method will elucidate the improvement and development of animal models of hypertension, and enhance the assessment of experimental therapeutic modalities.

Introduction

The importance of understanding the pathogenesis of hypertension is undisputed, and despite recent decreases in mortality due to heart disease and stroke, the burden of disease remains high. Based on data from 2018, 33% of adults in North America have hypertension, but only 53% of those with documented hypertension have their condition controlled to target levels[1]. An important feature of hypertensive angiopathy is vascular remodeling: a complex structural and spatial modification in small arteries that is of crucial functional consequence since it alters peripheral resistance and impairs contractility[2],[3],[4],[5].

The features of arterial remodeling in hypertension have been extensively studied[3],[4],[6],[7]. To date however, there are no data demonstrating how arterial remodeling in spontaneously hypertensive rats (SHR) is distinct from hypertension due to angiotensin II or deoxycorticosterone acetate infusion, inhibition of nitric oxide synthesis, or Goldblatt's model. The utility of animal models must be based on their resemblance to human pathology, yet commonly used measures are unable to quantify how arterial remodeling in experimental animals corresponds to arterial remodeling in humans. Thus, the well-established clinical

concept of target organ damage in hypertension[8] has yet to be supported by data indicating that arterial remodeling is more extensive in the kidney or heart, for example, compared to the skin, liver, or other organs.

In the majority of studies complex three-dimensional (3D) intra-organ arterial trees have been quantified by simple measures first described more than 80 years ago[9], consisting of the wall-to-lumen ratio (WLR), and/or the mean values for a variety of arterial dimensions, e.g., external diameter (ED), internal diameter (ID), wall thickness (WTh), external perimeter (EP), internal perimeter (IP), media cross sectional area (MCSA), lumen cross sectional area (LCSA), total cross sectional area (TCSA) and internal radius (IR). These measures are highly variable and inconsistent, and do not permit comparison of remodeling between different organs, hypertension models or species. Presumably, that quantification of tapered 3D intra-organ arterial trees on tissue sections is oversimplified, and conventional averaging of dimensions in vessel morphometry led to incomparable stochastic results. Modern micro-computed tomography achieves 3D images of peripheral vessels with high resolution: ~ 2.5 µm voxel size. However, in this technique, detailed microstructure cannot be described since only the contrast-filled lumen is visualised. While this is useful for angiogenesis studies, analysis of hypertensive remodeling is limited[10].

Arterial wall remodeling patterns have been classified as hypertrophic, hypotrophic or eutrophic, associated with inward narrowing or outward widening of the lumen[6],[11]. To date, however, there is significant discrepancy with regards to the type of remodeling that develops in terminal arteries (TAs) of different organs in various hypertensive models. In SHR for example, renal arterioles may demonstrate remodeling characterized as outward hypertrophic[12],[13],[14], inward hypertrophic[15], solely hypertrophic[13] or no

change[14],[16]. Some authors conclude that renal arteries > 60 µm do not develop remodeling[17], while others suggest an absence of remodeling for smaller arteries < 60 µm[16]. Mesenteric arteries may show inward hypertrophy or no change[12],[18]. Similar apparent contradictions appear in other hypertensive models[19],[20],[21],[22].

Such discrepancies could arise since arterial remodeling has previously been classified using empirical drawings, without precise quantitative analysis[11]. Since it was introduced twenty years ago, the classification has been extensively reviewed[5],[23],[24],[25] but has not been challenged with quantitative methods. Furthermore, frequently used parameters, such as WLR, remodeling index (RI), and growth index (GI) have not been rigorously tested as markers of remodeling. We therefore set out to i) study the classification of arterial remodeling patterns in hypertension, using mathematical methods, and ii) elucidate how arterial remodeling differs across a variety of organs. An algorithm for arterial remodeling assessment was developed, and we then determined if it could distinguish variants of remodeling in different organs within one model of hypertension in Goldblatt one-kidney one-clip (1K1C) rats. We hypothesized that, if conventional averaging was avoided, all organs would show the same arterial remodeling pattern. We also hypothesized distinct remodeling patterns for the adrenal gland and kidney, where the 1K1C model creates particular hemodynamic conditions. In this model, arteries within the adrenal glands experience the effects of an activated renin-angiotensin system (RAS), similar to other organs, but also experience enhanced flow due to diversion of blood from the main renal artery as a result of distal stenosis or ligation, similar to hemodynamic models of overflow[26],[27]. The remaining kidney also experiences the vasoconstrictive effects of an activated RAS, but under low blood flow due to the clipped renal artery[28],[29], that corresponds to low blood flow models[26],[30].

We also determined if examination of random tissue sections can provide useful information in studying hypertension, compared to use of arterial myography[3],[31]. In this regard, the vast majority of data from *in vitro* myography experiments has been generated from dissected mesenteric arteries, and may not be applicable to other organs. Finally, studies have recommended that arterial morphometry should only be performed on perfusion-fixed organs with pharmacologically relaxed vessels[31],[32]. We therefore examined if routine immersion fixation is appropriate for arterial remodeling analysis to elucidate comparisons between animal and human samples, since for the latter immediate relaxation and perfusion fixation are not practical in general.

Results and Discussion

Part I. Quantification of arterial trees on histological sections

Means of linear sizes and ratios are not applicable for arterial morphometry on tissue sections

While the parenchyma of different organs is well represented on histological sections, arteries are an exception. They appear as circles and irregular strips with a wide range of sizes and shapes, which are difficult to quantify[33]. To date, there are two approaches to arterial morphometry. *In vitro* myography uses similar vascular segments to minimize variability and allow comparison of averaged dimensions or their ratios among different models, or different arteries in the same model[34],[35]. However, myography data are restricted to only a few areas that are suitable for sampling - mainly the mesentery and aorta. Second, quantification of intra-organ arteries is based on casual measurements of arterial segments on tissue sections. However,

the majority of studies simply average the sizes and ratios, as for myography data, resulting in a high degree of variability and difficulty in comparing organs. Measured vessels are defined with uncertain ranges. For example, for the kidney: 'arteries and arterioles'[36]; 'intrarenal'[37],[38]; 'proximal interlobular'[13],[39]; 'afferent arterioles'[40],[41]; 'vessels adjacent to glomeruli in the outer cortex'[42] or 'at the same level proximal one-third from corticomedullary junction'[43]. Similar 'interlobular arteries' could vary significantly in ID (~100 μm[44], ~40 μm[13], ~25-50 μm[45], ~30-250 μm[22]).

TAs from multiple organs in normal rats were first analyzed using that conventional approach with measurements of mean ED, ID, WTh and WLR (**Table 1**). All values were obtained within an arterial ED range of 10-50 μm, since larger or smaller arteries were difficult to find in sufficient numbers in tissue samples. TAs in each organ were characterized by distinct average linear dimensions and WLRs. For instance, although bronchial and skeletal muscle arteries demonstrated similar WLRs, their EDs, IDs and WThs differed ($P < 0.01$). The WLRs for brain arteries were lower but IDs larger than in liver arteries ($P<0.001$), although EDs and WThs were similar between these two organs. Importantly, coefficient of variation of arterial dimensions were relatively high, varying between 40-70%, indicating their significant diversity[46]. Accordingly, individual histograms for parameter distribution in each organ were prepared. Histograms for ED, ID, and WTh demonstrated considerable variability, without a normal Gaussian distribution (**Fig 1**). Indeed, as shown in **S1 Table**, the extent of variability for ED, ID and WLR measures did not pass conventional statistical tests for normality.

Table 1. Averaged linear dimensions and wall-to-lumen ratio for terminal arteries with ED of 10 – 50 µm in different organs.

Organ	ED, µm	ID, µm	WTh, µm	WLR, %
Liver (N=63)	21.6±1.4	8.8±0.8**	6.4±0.4	98.6±7.2**
CV	54%	69%	48%	58%
Adrenal (N=61)	22.0±1.1	8.7±0.5	6.6±0.4	81.9±5.1
CV	40%	41%	52%	48%
Kidney (N=148)	32.7±0.6	13.3±0.4	9.7±0.2	78.9±2.2
CV	24%	33%	24%	35%
Skin (N=225)	20.1±0.6	8.5±0.3	5.8±0.2	75.3±1.9
CV	48%	52%	52%	37%
Skeletal muscle (N=98)	19.7±0.7*	8.4±0.3*	5.6±0.2*	70.8±3.1
CV	37%	37%	45%	43%
Bronchial arteries (N=50)	37.1±1.3	18.4±1.2	9.4±0.4	68.7±7.5
CV	24%	48%	32%	77%
Heart (N=115)	26.6±0.9	12.7±0.6	6.9±0.3	63.6±3.0
CV	40%	52%	42%	50%
Spleen (N=203)	17.7±0.5	8.3±0.3	4.7±0.1	61.6±1.3
CV	42%	51%	38%	30%
Small Intestine (N=55)	18.9±1.	9.5±0.8	4.7±0.2	57.2±3.0
CV	42%	65%	38%	39%
Stomach (N=90)	24.9±1.0	12.7±0.6	6.1±0.3	53.5±3.0
CV	41%	46%	54%	54%
Brain (N=144)	23.4±0.6	12.7±0.4	5.4±0.2	45.6±1.7
CV	32%	40%	35%	46%
Pulmonary arteries (N=66)	29.2±1.3	20.9±1.0	4.1±0.2	21.9±1.1
CV	35%	41%	34%	42%

Data are mean ± SEM. CV - coefficient of variation; N - number of measured arteries; *P<0.01 vs the bronchial arteries; **P<0.001 vs the brain. Organs are displayed in order of descending WLR values.

Fig 1. Detailed statistical analysis of primary data. Histograms for ED, ID, and WTh in the kidney, heart and pulmonary arteries, used to calculate statistics in Table 1, demonstrated irregular frequencies and profound asymmetry.

Our detailed analysis (**Table 1, Fig 1, S1 Table**) indicates that mean values have little statistical value with regards to such measurements[46], since even a small range of EDs (10-50μm) for TAs in all organs was associated with an abnormal distribution and high variability. Furthermore, increasing numbers of measurements to normalize distribution and reduce variability are not effective for tapering branching objects[33].

While WLR is considered independent of diameters and not affected by the size of arteries studied[3],[9],[41], this matter has not been rigorously substantiated in the literature[4],[5],[25],[32],[47]. Furthermore, we found as many as sixteen different formulae to calculate WLR. Some studies employed the diameter or radius: WTh/ID[20],[44],[48]; ED - ID/2ID[49]; ED/ID[50]; WTh/IR[12][17]; a media index WTh/IR with IR specifically defined as the distance from the center of the arterial lumen to the middle point of the media[51]; 2WTh/ED[52],[53]; 2WTh/ID[54]; WTh/ED[55]; or ID/ED[56]. Others have measured WLR from the perimeters as EP/IP[40],[41],[42], or preferred to use the area: MCSA/LCSA[15],[16],[45]; MCSA/TCSA[37]; LCSA/MCSA[36]; LCSA/TCSA[57]. The WLR has also been interpreted as the ratio of the area to perimeter MCSA/IP[22], or renamed RI[58]. Rarely, point counting has been used to estimate WLR as the average ratio of the volume density of the walls to the volume density of the lumens[16],[59]. However, many studies indicate that WLR is not constant but declines 2-10-fold in arteries of ED 20-500 μm in the

human and rat kidney[51],[60]; human and rat brain[61],[62]**; a**nd human and dog liver[48],[63]. Our data indicate that WLR is not constant even within a small range of EDs (**Fig 2A)**.

Fig 2. **Detailed statistical analysis of primary data.** (A) WLR scatterplots were irregular with low r^2 (solid lines), and wide 95% prediction bands (dashed lines). Corresponding statistics are shown in **Table 1**. (B) Scatterplots of primary data displayed certain incremental change in arterial dimensions. Coefficients r^2 were moderate, and the pulmonary arteries had the best fitting value.

In summary, neither averaged WLR nor the mean values for ED, ID or WTh are applicable to even relatively small intervals of vessel caliber. Thus, any comparison of mean values for these measures is not appropriate[46].

Application of short intervals provides precise complex profiles and linear regression equations

For vessels with EDs in the range of 10-50 μm, there was a trend towards dependence of ID and WTh on ED, although variability was substantial (**Fig 2B**). We therefore assessed primary data with a complex profile method, which is widely used in cartography, thermodynamics, and engineering[64],[65]. In this technique, a contour line is drawn as a function of two variables, where the gradient of function is perpendicular to the contour isoline, thus representing more than two dimensions on a two-dimensional (2D) graph. To be applied to measuring arteries, each arterial circle on a histological section is first characterized by three values: ED, ID, and WTh. Then all measured vascular circles were arranged in a row in order of ascending ED, and numbered from 1 to N, where N is the total number of measured arterial rings. Subsequently,

each number was plotted on the y-axis, while its corresponding ED, ID and WTh were plotted on a bidirectional x-axis (**Fig 3**).

Fig 3. Analysis of primary data with complex profiles. Primary measurement for the kidney, heart, and pulmonary arteries were arranged in the complex profiles. Axis X – the bidirectional common scale for ED (outer contours), ID (inner contours), WTh (shaded regions); axis Y represents the number of measured arteries (variables) in order of ascending ED. Steps in the outer contours (solid arrows) reflected a minimal division on an eyepiece micrometer. Outliers along the internal contours (dashed arrows) corresponded to wider or narrower ID, compared to neighboring ED values.

The same primary data, represented in this way, revealed a regular hemodynamic structure. Staircase steps of the external contours were relatively small and regular since a conventional microscope with a 40x objective provided a minimal division value of ~2 μm to the eyepiece micrometer, so that each ED was rounded off to ± 2 μm. Spikes of internal contours were larger and quite irregular corresponding to some arterial segments with similar ED but different ID and/or WTh, and it was necessary to understand the source of multiple outliers. Presumably, those outliers represented subsets among arterial segments, branching at different hydrodynamic points. We speculated that arteries with similar ED at proximal regions should have thicker media, i.e. higher wall-to-lumen ratio, in response to larger pressure gradients (**Fig 4A**).

Fig 4. **The hemodynamic explanation for the appearance of outliers.** (A) According to Fick's law, the capillary pressure in proximal (p1) or distal (p2, p3) regions must be similar, while

arterial pressure in a proximal artery P1 is higher than in distal arteries P2 and P3. Consequently, $\Delta(P1- p1) > \Delta(P3 – p3)$. Arteries at proximal regions should have thicker media, i.e. higher wall-to-lumen ratio, in response to larger pressure gradients. (B) The paired sampling of pulmonary arteries. Forty five arterial pairs with the same ED were identified in the proximal axillary and distal dichotomous branches respectively. For example, A1 (the red bar) and A3 (the green bar), sampled into paraffin blocks, and dimensions were measured on stained sections. Scale bar, 100 μm. (C) Five pairs in the table are the examples of the total (N=45) measured pairs of branches with the same ED that could have differences from 50-110% in ID, 100-230% in WTh, and 250-600% in WLR ($P<0.001$). (D) In the complex profile, those neighboring branches create most outliers, as in **Fig 3.**

To test this hypothesis, dissected pulmonary arteries were measured by the paired sampling: branches of the same ED were identified in the proximal and distal segments, cut at branching points, and their dimensions were measured (**Fig 4B-D**). To compare only two vessels 5 mm apart would require enormously laborious reconstruction of approximately 2000 serial sections while the method of paired branches morphometry was much more effective. Axillary and regular dichotomous branches with the same ED but smaller ID and thicker WTh would be placed closer in profiles, determined as outliers (**Fig 3**). That explained the presence of numerous outliers as an intrinsic property of arterial branching to respond to variable local hemodynamics, that complies with a conception of constrained random branching for smaller vessels [66]. Outliers are not evident in primary data plots (**Fig 2**) to be removed. Moreover, a conventionally recommended increase in number of measurements[46] simply increases the number of outliers.

To make outliers more evident, instead of conventional averaging of the data for the entire range of 10-50 µm, the ED was divided into short regular intervals (**Fig 5**).

Fig 5. Basic approach to arterial morphometry analysis. (A) In the conventional approach, statistics of arterial dimensions are calculated for a broad range of calibers. (B) In the proposed algorithm, statistics are calculated for fixed 5µm intervals for TAs with ED ~ 10-50 µm.

To avoid averaging, some investigators have measured interval means. However, significant discrepancies in choice of interval steps and caliber ranges render such data as highly variable and difficult for comparative analysis. Some studies considered two intervals as 'interlobular and arcuate' with ID ~ 70 and ~160 µm[59], or 'small and intermediate' as ED~ 50-100 and 100-500 µm[60]. Others found it more appropriate to divide 'interlobar vessels' into six intervals of <70, 70-95, 95-120,and >120 µm[16]. Another variant was to cut the range of 90-220 µm into four equal classes[21]. A choice for cerebral arteries was four intervals of IR <20, 20-49, 50-79, and >80 µm but for older animals it was only 2 of 80-119 and 120-159 µm[61]. A different subdivision was used for the liver: ≤ 20, 21-50, 51-124, and > 125 µm[48]. In the lung seven non-regular intervals of 0-50, 50-100, 100-200, 500-1000, and >1000 µm were counted[53]. Thus the advantage of using intervals could be compromised by subjective choices of interval size that neither improves standardization nor comparison.

We tested different intervals, and found that the interval of 5 µm was optimal for all organs. That interval corresponds to adding one layer of vascular smooth muscle cells, which has a normal thickness of 5-7 µm[63],[67]. Indeed, the relation between WTh and the number of VSMC-layers can be represented by a linear regression line (r = 0.88)[63].

When the complex profiles had been drawn not from every measured value, but from the mean interval values, they demonstrated organ-specific gradients in tapering (**Fig 6A, S1 Fig**) allowing comparison of arterial remodeling between organs. Furthermore, in contrast to data depicted in **Fig 2B**, if outliers had been removed, the means of short intervals revealed very tight linear regression between both lumen and wall thickness and vessel caliber in kidney, heart and pulmonary vessels, and in other organs as well (**Fig 6B, S2 Fig).** All acquired equations demonstrated goodness of fit coefficients r^2 between 0.8 - 0.9 ($P < 0.0001$), with few exceptions for WTh in the brain and bronchial arteries (**S2 Table**).

Fig 6. Application of the short fixed intervals significantly improved primary data analysis. (A) Complex profiles were built from the accumulated frequencies (axis Y) of the means of ED, ID, and WTh for 5-μm ED intervals. In contrast to scatterplots in **Fig 2B**, terminal arteries exhibited distinctive tapering patterns in organs. Complementary graphs are in **S1 Fig.** (B) Mean values of ID and WTh for the regular 5-μm ED intervals revealed robust linear regression equations ($P<0.001$). Complementary graphs are in **S2 Fig.** Points on the lines are mean ± SD for 5-μm ED intervals.

To decide whether linear regression equations for TAs were organ-specific, their slopes and intercepts were compared. Equations for pulmonary, bronchial, adrenal, stomach and skeletal muscle TAs were distinct ($P<0.0001$). Heart and spleen TAs had similar equations, as did brain and intestine, and kidney, liver, and skin (**S3 Fig**).

Only a few attempts to apply linear regression to arterial morphometry have been published[18],[22],[51],[63]. Those studies demonstrated that the range of EDs from 10-100 μm

fits linear regression, while wider intervals of ED 100-1000 μm follow an exponential function. We found the range of EDs from 10-50 μm was the most practical to analyze. That caliber is not only the most frequently observed, but also best addresses the functional consequence of remodeling, being responsible for maximum values in peripheral resistance[3],[4],[5].

The same calculation, based on means of short intervals, was applied to compute WLR, although the ratio continued to demonstrate high variability (**Fig 7A**), presumably due to the interaction of standard deviation in the ratio of two dependent values[46]. It is evident, comparing different organs, that irregular graphs of mean interval WLRs are difficult to approximate correctly (**Fig 7B**). Therefore we calculated interval WLR from verified linear regression equations (**S2 Table**). The results demonstrated clearly that WLR is not constant, with evidence for nonlinear increases or decreases (**Fig 7C)**.

Fig 7. Significant variability of the wall-to-lumen ratio in different organs. (A) Interval means of WLR still varied significantly, although r^2 improved as compared with **Figure 2A** (P ≈0.14-0.02). The pulmonary arteries had the highest r^2 fitting value (P=0.002). Points on the lines are mean ± SD for 5-μm ED intervals. (B) Means of WLR for the 5-μm ED intervals were irregular, except in pulmonary arteries. (C) WLRs were counted from the linear regression equations. The ratios were not constant, decreasing or increasing by nonlinear functions.

Hemodynamic significance of morphometry data

Reliable linear regressions also validated an assessment of relative resistances (RR) that was calculated using Poiseuille's relationship $RR=1/\pi r^4$, assuming constant viscosity and length, and where r is the radius of the vessel lumen, as it was recommended[63],[68],[69]. RRs for 5 μm regular intervals across multiple organs are depicted in **Fig 8 and S2 Fig**, with the highest values

in liver, and lowest in pulmonary arteries, rising exponentially in the smaller segments, since blood flow is proportional to the fourth power of the luminal radius.

Fig 8. Comparative analysis of the relative resistance in different organs. (A) RR curves were calculated from the regression equations in **S2 Table**. The liver and spleen had the largest values (P<0.001), while the pulmonary and stomach arteries - the lowest (P<0.001). (B) Diversions in RRs were better revealed on the logarithmic scale.

Accordingly, terminal relative resistance (TRR) would estimate the resistance for the smallest vessels of ED= 10-20 μm that have the largest accumulated frequency in complex profiles (**Fig 9A**).

Fig 9. Correspondence between morphometric and hemodynamic parameters. (A) TRR demonstrated similarity in organ-to-organ ratio with vascular resistances acquired with physiological methods: modified from[70] (B); [71](C);[72] (D). Data on (A) are mean ±SEM, on (B-D) – mean values.

Since the complex profiles reveal the average numbers of arterial branches of defined lumen diameters in each organ, prior to the capillary bed, it would be reasonable to measure terminal capacity (TC) in each organ, as the sum of the internal volume of each segment multiplied by its frequency:

$$TC = \sum(\pi * (\mathbf{ID}i)^2 /4)i\% \qquad (1)$$

Where **ID***i* is the mean ID of each interval, calculated from the linear regression equation; *i*% - the frequency of that interval in the complex profile (**Fig 10A).**

Fig 10. Correspondence between morphometric and hemodynamic parameters. (A) TC values were in good agreement with organ blood flow rates, estimated by a physiological method[73] (B). Data on (A) are mean ±SEM, on (B) – mean values.

The hemodynamics of each organ are characterized by blood flow rate (BFR), regional vascular resistance (RVR), vascular volume, and percentage of cardiac output received[70],[71], reflecting the uniqueness of a vascular bed. Although each organ possesses a distinctive arterial tree, there are currently no standardized morphometric parameters to quantify those distinctions and correlate them to BFR or RVR[68],[69]. Indeed averaged EDs, IDs, and WLRs are only loosely associated with hemodynamic parameters, although they accompany impaired contraction or relaxation in *in vitro* myography experiments[62]. Our algorithm provides a promising solution to this problem. The use of linear regression equations allows for quantification of TRR, which reveals significant similarity to RVRs obtained by physiological methods (**Fig 9B-D**)[70],[71],[72]. The proposed TC formula also shows good correlation with BFR, determined by microsphere method[73] (**Fig 10**).

Larger arteries are the most important source of errors

In TAs with ED > 40 μm, only a small number of measurements per interval could be obtained that has a crucial impact on the precision of regression equations, since even one outlier can alter the result significantly, i.e. the means of such intervals are unreliable[46], and therefore the same data set could be approximated with several equations and RR curves, depending on numbers of

counted larger vessels (**Fig 11**). Small deviation of regression lines significantly affect RR according to the formula $R= 1 /\pi r^4$. In our study, minor deviations of 8-12% in the largest IDs caused deviations of 25-90% in the smallest IDs, which in turn, had pronounced effects on the calculated TRR values, since blood flow is proportional to the fourth power of the luminal radius. To avoid such errors, the equations must be verified by comparison of corresponding RR curves (**Fig 11**).

Fig 11. The equations must be verified to avoid the effect of fewer data points for larger vessels. (A) Heart. Means of intervals were approximated with two equations to compute RR curves. The first (red formula and lines) accounted for vessels of ED 10-50 μm. The second (blue formula and lines) accounted for all vessels found (ED=10-120 μm), with only 1-3 values per interval for the largest TAs. The equations were highly distinct between each other ($P<0.001$), and every line and curve had the highest goodness of fit coefficient r^2 and $R^2 \approx 0.98$-0.99. (B, as boxed area in A) For the smallest arteries, the difference in ID of 1-2 μm (arrows) resulted in a 270% difference in RR curves ($P<0.0001$). If the RR curve was calculated not from the equation but from means of intervals (green line), it was closer to the red ($P>0.88$) than to the blue curve ($P<0.0001$), i.e. the equation for 10-50 μm (red) was correct. (C,D) The same calculation for intestine. The equation for 10-70 μm was correct ($P>0.90$ vs $P<0.22$). Points on the lines are mean ± SD for 5-μm ED intervals, n – number of measurements per interval

The method enables comparison between species

Using this approach, we compared TAs between normal rat and mouse. While averaged dimensions demonstrate no substantial differences, the complex profiles, linear regression equations and RR curves revealed specific patterns for each species (**Fig 12**). In rats renal TAs

have thicker media and narrower lumens compared to mice, but lower resistance, which is consistent with hemodynamic data[74].

Fig 12. **The algorithm enables comparison between species.** (A) Scatterplots for ED, ID, and WTh for the rat and mouse. (B) Mean values from scatterplots revealed no difference **(**P>0.40), including WLR. The corresponding complex profiles (C), and regression equations with the relative resistance curves (D) were very distinctive (P<0.001) for the rat (dashed line) vs mouse (solid line).

Part II: recognition of remodeling patterns in hypertensive rats on histological sections

Conventional measurements exhibit different remodeling patterns in hypertensive rats

At 60 days, the systolic blood pressure in the sham-operated and hypertensive rats was 115±6 mmHg and 217±21 mmHg, respectively (P<0.001). Morphometry data from multiple organs were first analyzed using conventional measures of mean ED, ID and WTh for the arterial ED interval of 10-50 μm. 1K1C hypertension significantly affected TAs in every organ (**Table 2**).

Table 2. The spectrum of remodeling variants in terminal arteries of ED 10 – 50 µm.

Organ	Sham rats			1K1C rats			WLR	MCSA	NC
	ED, µm	ID, µm	WTh, µm	ED, µm	ID, µm	WTh, µm			
Brain	23±7	13±4	5±2	19±8**↓	7±4**↓	6±2 *↑	↑	↓	**3-4cI**
Kidney	33±8	13±4	10±2	30±9**↓	10±4**↓	10±3 =	↑	↓	**3-4b**
Heart	27±9	13±6	7±3	27±10 =	11±4**↓	8±3*↑	↑	↑	**2-4c**
Pulmo-nary	29±8	21±8	4±1	33±9**↑	22±6 ↔	6±1**↑	↑	↑	**1-5c**
Skin	20±9	8±4	6±3	23±9**↑	8±3 =	7±3**↑	↑	↑	**1-5c**
Skeletal muscle	20±7	9±4	5±3	21±10 =	8±3**↓	6±3 **↑	↑	↑	**2-4c**
Bron-chial	37±9	18±7	9±1	32±10**↓	13±6**↓	10±2**↑	↑	↓	**3-4cI**
Stomach	25±7	13±5	6±3	27±11*↑	10±5**↓	8±3**↑	↑	↑	**1-4c**
Intestine	19±8	9±6	5±1	24±10**↑	9±4 =	7±3**↑	↑	↑	**1-5c**
Adrenal	22±8	9±3	6±2	24±11**↑	14±5**↑	5±3*↓	↓	↓	**1-6aII**
Liver	22±9	8±4	6±2	22±12 =	7±4 =	7±3 =	=	=	**2-5b**

Data are mean±SD. *P<0.05; **P<0.01 NC, numerical classification. ↑ ↓ = indicate increase, decrease or no change respectively vs control values.

To date, the majority of studies use the widely accepted classification[11] **(Fig 13).** However, the obtained remodeling varieties did not fit into conventional definitions. The classification considers 'inward' or 'outward' as only simultaneous ED-ID decrease or increase (**Fig 13**). The brain, bronchial and kidney should be named 'inward hypotrophic' due to reduced ED, ID and MCSA, but that term does not mark increased or stable WTh. The classification has no 'inward-outward hypertrophic' type that appeared in means for the stomach. The heart and skeletal muscle should be defined as 'inward' because mean IDs were reduced, but constant mean EDs are not recognised, there is no 'inward-only hypertrophic.' The same for constant IDs in the pulmonary, skin and intestine, that should be classified as 'ourward-only hypertrophic.' For unknown reason, the remodeling had been considered only as keeping constant MCSA, and not constant WTh. The results were based on averaged linear dimensions, and hypertensive values demonstrated a high degree of variability and abnormal distribution (**S4 Fig**). Accordingly, conventional averaging of dimensions led to the designation of diverse remodeling patterns.

Fig 13. The descriptive conventional classification[11]**.** The 'inward' or 'outward' means reduction or increase in lumen; the 'hypertrophic,' 'eutrophic,'and 'hypotrophic' indicates increase, no change, or decrease in wall cross-sectional area, respectively.

There is a general assumption that in humans and animals, regardless of the type of hypertension, small arteries develop inward eutrophic or inward hypertrophic remodeling[7],[24]. Other studies have suggested that inward eutrophic remodeling occurs in essential hypertension, while secondary hypertension is associated with hypertrophic remodeling[4]. The concept of uniform remodeling is logical and reasonable since arteries throughout the body have similar structure

and regulatory mechanisms. Nevertheless, studies using either random sections or *in vitro* myography present an entire spectrum of possible remodeling patterns. Differences in animal age, heterogeneous post-mortem arterial contraction, variable perfusion pressure, and different histoprocessing and morphometry techniques may account for data inconsistency[3],[47]. However, our attempt to find uniform remodeling in 1K1C rats by using the same tissue preparation and morphometry technique simultaneously in ten organs failed, and instead revealed distinctive, and even opposite patterns (**Table 2**).

Many authors have presented data avoiding classification[14],[75],[76],[77]. Reviews on this subject have focused on the method of tissue preparation and the potential for sampling bias, and the general approach has not been revised[3],[24],[25],[31]. Indeed, the conventional classification was based on sketch-drawings, with assumptions regarding geometric parameters[11] (**Fig 13).** The classification presumed, for unclear reasons, the simultaneous movement of ED and ID as inward or outward. Such movement would occur if the artery remodeling is considered as simple inflation or deflation for an elastic, homogenous, gel-like structured thick-wall cylinder[78],[79]. However, the arterial wall is categorized as a multilayered, helically arranged, fiber reinforced composite, with independent ED vs ID displacement[80]. Wall remodeling is therefore a multilayered interaction involving hypertrophy[81],[82], hyperplasia[21],[83], apoptosis[81], hyalinosis and fibrinoid necrosis[84], [85] of vascular smooth muscle cells, as well as deposition of extracellular matrix[86],[87]. The extent of these changes varies from inner to outer layers[88],[83],[76]. We also have found that quite often statistical data from studies could not be even assigned to a certain type because statistical casualties break geometry rules. For example, mean ED and ID remains constant but WTh increased[60], mean ID decreased while MCSA and WTH remain constant[89].

471

472 **The conventional classification is unable to categorize remodeling variants**

473 In order to precisely categorize remodeling variants in consideration of the conventional
474 designations of inward-outward and hypertrophic-hypotrophic (**Fig 13**), possible conformations
475 of a blood vessel were modeled with the approximation of arteries as thick-wall cylinders
476 capable of changing ED and ID independently (**Fig 14).**

477

478 **Fig 14. Numerical modeling approach.** (A) For numerical modeling the ED (2) and ID (5)
479 changes independently. ED could moves outward (vector 1) to increase ED or inward (vector 3)
480 to reduce ED. ID could shift inward (vector 4) to decrease ID or outward (vector 6) to increase
481 ID. (B) An example of numerical classification. The number 1, 2 or 3 indicates increased (↑),
482 stable (=), or reduced (↓) ED respectively. The number 4, 5 or 6 reflects decreased, constant or
483 increased ID. The letter a, b or c identifies diminished, constant or increased WTh. White
484 semicircles – control, black – predicted remodeling variants.

485

486 In a simulation procedure, each variant was considered distinct if a value for only one dimension
487 in the set of five (ED, ID, WTh, MCSA, WLR) was different from the value for another set. The
488 numerical modeling (**Fig 15**) revealed not six, as empirically suggested, but twenty variants of
489 arterial remodeling. For example, increasing ED produces eight (1-4, 1-5, 1-6aI, 1-6aII, 1-6b, 1-6
490 cI-cIII) possible variants by combination of changing ID, WTh and MCSA in different
491 directions. A constant ED results in two variants (2-4, 2-6), and decrease in ED generates nine
492 variants (3-4 aI-aIII, 3-4b, 3-4 cI-cIII, 3-5, 3-6). Variants 1-6 cI-III, 3-4 aI-III and 3-4 cI-III are
493 possible because not only the direction but even gradients of change between ED and ID could

elicit unique remodeling patterns, which were impossible to classify with conventional definitions.

Fig 15. The formalization of numerical modeling for predicted remodeling variants. The number **1, 2** or **3** indicates increased (↑), stable (=), or reduced (↓) ED. The number **4, 5** or **6** corresponds to decreased, constant or increased ID. The letter **a, b** or **c** identifies increased, constant or diminished WTh respectively, for the same set of ED and ID. The additional Roman numerals **I-II-III** detail the dynamics in MCSA and WLR for the same set of ED, ID, and WTh due to possible gradients in ED vs ID displacement. The 2-5b variant indicates no remodeling. White semicircles – control, black – predicted remodeling variants.

Therefore, the conventional term "hypertrophic" would equally apply to nine variants: 1-4, 1-5, 1-6cI-III, 2-4, and 3-4cI-III. The term "outward" would cover simultaneously 1-4, 1-5, and all six sub-variants 1-6. The term "eutrophic" would equally apply to 1-6b, 3-4b or 3-4cII, while "hypotrophic" could be true for 1-6aI-II, 2-6, 3-4aI-III, 3-5, and 3-6. According to this numerical classification, in 1K1C rats TAs demonstrated seven remodeling variants across organs (**Table 2)**. Studies using either random sections (**Table 3**) or *in vitro* myography (**S3 Table)** are also very inconsistent.

517 **Table 3. Numerical classification applied to arteries studied on random histological**
518 **sections.**

References	Experimental model	Arterial location	NC
Liu et al.[17]	2K1C (PF)	renal arterioles 30-60µm > 60µm	**2-4c** **2-5b**
Helmchen et al.[44]	2K1C (IF)	interlobular	**1-5c**
Qin et al.[82]	2K1C(PF)	mesentery	**1-4c**
Korsgaard et al.[90]	1K1C, unfixed, wire myograph	mesenteric III branch renal arcuate arteries	**3-4cIII** **2-5b**
Deng et al.[77]	wire myograph, 2K1C 1K1C	mesentery III order mesentery III order	**3-4cIII** **3-4cII**
Zhou et al.[87]	2K1C, wire myograph	renal arteries	**3-4cIII**
Kinuno et al.[13]	SHR (PF) SHR+uninephrectomy (PF)	renal interlobular renal interlobular	**1-5c** **1-6aII**
Owens et al.[18]	SHR (PF)	mesentery, I branch II branch III - IV branch	**3-4cII** **2-5b** **3-4cIII**
Smeda et al.[16]	SHR (PF)	renal, ID~20-60µm renal, ID~300-60µm	**2-5b** **1-5c**
Johansson B.[91]	SHR (PF) SHRSP (PF)	cerebral extracranial cerebral intracranial cerebral extracranial cerebral intracranial	**1-6cI** **1-5c** **1-6cIII** **1-6aII**
Nordborg et al.[12]	SHR (IF) SHRSP (IF) SHR (IF) SHRSP (IF)	IF, mesentery mesentery renal renal	**3-4cIII** **3-4cII** **1-5c** **1-6cI**
Leh et al.[14]	SHR (IF)	renal afferent arterioles	**1-6cI**
Ohara et al.[15]	SHR (PF)	PF, renal interlobular	**2-4c**
Kost et al.[92]	SHR (PF)	renal afferent interlobular arcuate	**2-5b** **2-5b** **3-5a**
	SHR+AngII (PF)	renal afferent interlobular arcuate	**2-5b** **1-5c** **1-5c**
Lee et al.[47]	SHR (PF)	mesentery, ID~120-250 µm	**1-5c**
Limas et al.[50]	SHR, age dependent (PF) renal, ED~50-100 µm	10 weeks 20 weeks 28 weeks 48 weeks	**2-5b** **1-5c** **3-4b** **2-4c**
Casare et al.[19]	AngII (PF)	renal afferent interlobular	**1-6cII** **1-6aII**
Berry et al.[21]	DOCA (PF) intrarenal,	ED ~ 400-500µm ED~ 200-300µm	**1-6cI** **1-5c**
Mazzali et al.[40]	Hyperuricemia (IF)	renal afferent arterioles	**1-4c**

519 2K1C, two kidney-one clip; Ang, angiotensin; DOCA, deoxycorticosterone acetate; IF,
520 immersion fixed; PF- perfusion fixed; SHRSP – spontaneously hypertensive rats stroke prone;
521 NC – numerical classification.

522 We have found only one study that applied a numerical approach to remodeling[31]. The
523 numerical classification proposed here unambiguously defines any wall conformation, and could
524 be applicable to remodeling not only in hypertension but diabetes, atherosclerosis[93],[94], high
525 or low blood flow[48],[27], restenosis[95], vasculitis[96], or bronchial remodeling[97].

526

527 **Remodeling patterns are not identified with WLR, RI or GI**

528 To decide whether remodeling varieties (**Table 2, 3 and S3 Table)** truly exist or are derived
529 from conventional averaging, we tested methods recognizing that arteries follow one of twenty
530 predicted variants.

531 Increased or decreased WLR is widely used as the main criteria of 'inward' vs 'outward'
532 wall conformation[3],[4],[5]. It is not appropriate because WLR could be similarly increased in
533 nine, decreased in eight, and unchanged in three variants. Therefore the frequently used WLR
534 could unambiguously define neither wall thickening nor lumen narrowing (**Fig 15**).

535 RI and growth index GI are also regarded as the main parameters to estimate
536 remodeling[35],[98],[24]. According to the primary data[6], basilar arteries in SHR developed
537 the variant 3-4cIII as a combination of hypertrophy and rearrangement (remodeling) of vascular
538 smooth muscle cells (**Fig 16**). The proposed combination was explained with two formulae. The
539 formula (1) below was based on the first presumption: what would the ID be if vessels
540 underwent the variant 3-4cII (ID*3-4cII*) i.e. hypertensive MCSA (MCSA*hr*) remains equal to
541 normal MCSA (MCSA*n*)? The formula (2) below was based on the second presumption: what
542 would the ID be if vessels developed the variant 2-4c (ID*2-4c*) i.e. hypertensive ED (ED*hr*)

remains equal to normal ED (ED*n*)? To create the formula (1), the larger MCSA*hr* was ignored in favor of a proposed MCSA*n*=MCSA*hr* to calculate percent of encroached lumen if the variant 3-4cII would occur:

$$\text{Percent of encroached lumen} = \frac{\text{ID}n-\sqrt{\text{ED}hr^2-4\text{MCSA}n/\pi}}{\text{ID}n-IDhr} = \frac{\text{ID}n-ID(3-4cII)}{\text{ID}n-IDhr} \quad (1)$$

For the formula (2), the smaller ED*hr* was ignored in favor of a proposed ED*n*=ED*hr* to calculate percent of encroached lumen if the variant 2-4c would occur:

$$\text{Hypertrophy} = \frac{\text{ID}n-\sqrt{\text{ED}n^2-4\text{MCSA}hr/\pi}}{\text{ID}n-\text{ID}hr} = \frac{\text{ID}n-\text{ID}(2-4c)}{\text{ID}n-\text{ID}hr} \quad (2)$$

The primary definition "percent of encroachment lumen" in the first formula was renamed the "remodeling index", and the second formula for "hypertrophy" was modified to "growth index" by[98]. Unlike the second formula, GI counted true MCSAs:

$$\text{GI} = \frac{MCSAhr-MCSAn}{MCSAn} \quad (3)$$

Accordingly, the formulae were intended to quantify only *a subjective interpretation* of 3-4cIII as a combination of 2-4c and 3-4cII but that interpretation could be valid as any combination between eight variants with diminished ID (2-4c, 3-4aI-III, 3-4b, 3-4cI-III). Therefore calculation of RI is also incorrect because the formulas were designated to analyze only the proposed combination (**Fig 16**).

Fig 16. **The first attempt to quantify remodeling**[6]. The reductions in both mean ED and ID were interpreted by the authors as a possible combination of hypertrophy (variant 2-4c) and rearrangement of vascular smooth muscle cells (variant 3-4cII). White semicircles – control, black – predicted remodeling variants

GI does not bear any information about growth, as it simply counts the percentage change in MCSA that could be assigned to different variants (**Fig 15**). This may account for the variable RI and GI values found in *in vitro* myography experiments, which are considered gold standard due to sampling of similar mesenteric arteries branches. According to formulae (1) and (2), the sum RI+GI must be 100%, but it appears only in the first authors' publication (**S3 Table**). The question still remains: how to recognize a particular remodeling variant?

Remodeling patterns are not identified on 2D graphs

The analysis of the simple annular ring in histological sections represents a conundrum, since arteries have no 'reference points' from which they have been modified to assume a remodeled shape (**Fig 17**). According to the literature and own data, any of the 20 predicted types of remodeling could occur (**Table 2, 3 and S3 Table**).

Fig 17. The conundrum in arterial remodeling assessment. Each artery could be an image of another one before or after remodeling: there is no "reference point" indicating its previous dimensions. Scale 10 μm.

As in control rats, primary measurements were organized in 5 μm intervals, the mean value for each interval was calculated, and the complex profile and linear regression equations built from the means of intervals (**S4 Table**). Data analysis revealed that comparison of complex profiles also could not be used to identify remodeling variants because it was complicated by the existence of uncertain starting points for superimposition of a hypertensive graph on the control one (**Fig 18A, S5 Fig**). Furthermore, there are no data indicating how vessel remodeling progresses in a length-wise fashion, except for the presence of increased vessel

589 tortuosity[29],[63]. While the common starting points were unclear, varying accumulated
590 frequencies suggested distinct remodeling patterns even in different segments within the same
591 organ (**Fig 18A, S5 Fig**).
592
593 **Fig 18. Considerations for arterial remodeling assessment.** (A) The profile of hypertensive
594 (red) renal TAs was superimposed on the control (green). The starting point (the curved arrow) is
595 uncertain: inward–outward remodeling (the solid double arrow) is well known, while proximal-
596 distal shifting (the dashed arrow) is unacknowledged. Uneven accumulated frequencies displaced
597 interval values irregularly. Complementary graphs are in **S5 Fig.** (B) Linear regression lines of
598 renal TAs demonstrated decreased ID (solid lines) and increased WTh (dashed lines) in
599 hypertension. The slopes were different ($P<0.0001$). Complementary graphs are in **S6 Fig**.
600
601 Next, we tested if linear regression could identify remodeling patterns. Compared to the
602 complex profiles, the linear regressions demonstrated smaller IDs and bigger WThs for the same
603 ED similarly in all organs, except the kidney and adrenal (**Figure 18B, S6 Fig**).
604 To understand how shifts in regression lines could verify remodeling, every predicted
605 variant, for each organ, was simulated from control linear regression equations (**S4 Table**). Some
606 studies considered that not WTh/ID but other ratios such as EP/IP[42],[41], or
607 MCSA/LCSA[13],[38],[45], or MCSA/IP[22] are more reliable and informative. Therefore we
608 tested all possible dimensions and their ratios to demonstrate the lack of reliability in 2D graphs.
609 Simulation was done for: linear sizes including ED, ID, WTh, internal perimeter (IP), external
610 perimeter (EP); areas, such as MCSA, lumen cross sectional area (LCSA), total area
611 (MCSA+LCSA), and ratios, including WLR, EP/IP, and MCSA/LCSA.

For all tested dimensions, the regression line displacement from the control line was similar for as many as 11 variants (**Fig 19, S7 Fig)**. Any linear size, area or their ratio exhibited similar displacement for many different remodeling variants. While the use of linear regression equations can verify the presence of remodeling, the equations are unable to define a specific remodeling pattern. Thus, it was not possible to distinguish arterial spatial conformations on routine 2D graphs.

Fig 19. Remodeling variants are not distinguishable in two-dimensional graphs. The simulated remodeling of renal arteries for the variants 1-4c, 1-5c and all 1-6. For any parameter a line shift was similar to others, and could distinguish only increase or decrease from control but not verify a particular pattern. MCSA - media cross sectional area, LCSA – lumen cross sectional area. Complementary graphs are in **S7 Fig**.

A method of 3D-modeling simulation recognizes remodeling type

A 3D-modeling simulation was applied to address the limitations with 2D graphs. There were four steps to this method. For example, for the brain, IDs and WThs were calculated from the control linear regression equations (**S4 Table**) and placed in 3D-graphs (**Fig 20, S8 Fig**). Then, IDs and WThs for each of twenty possible remodeling variants were computed from the control equations and added to the 3D graphs. Every remodeling pattern was simulated by calculating its possible maximal deviation in dimensions that were arbitrarily limited to 300% for wall thickening or lumen widening, and 99% for wall thinning or lumen narrowing. IDs and WThs were then calculated from the hypertensive regression equations (**S4 Table**) and also added to 3D graphs. Finally, line proximity between real and predicted values was verified with methods

of analytic geometry in 3D space[99]. From all possible variants the hypertensive remodeling in cerebral TAs corresponded only to the variant 2-4c.

Fig 20. 3D modeling simulation for the brain. In 3D graphs, the control equation (green lines) and each predicted variant (blue lines) are connected by the planes (grey) representing sets of all possible values that ED, ID, and WTh could acquire during transformation. The red lines represent the regression equation for hypertensive rats (**S4 Table**). The red lines were not congruent with any of the predicted planes, except for the variant 2-4c. The method readily distinguishes the gradients ΔED, ΔID, and ΔWTh for the variants 1-6 and 3-4 that could only be implied in 2D graphs in **Fig 19.** Axis X – ED, axis Y – ID, axis Z – WTh, μm. Complementary graphs are shown in **S8 Fig., S19 and S20 Video files**. Throughout the article**,** coordinates in some graphs were rotated at different angles to optimize display.

The brain, heart, lung, bronchi, liver, stomach, intestine, skin, and skeletal muscle developed the same remodeling variant 2-4c, supporting the concept of uniform remodeling (**Fig 21**).

Fig 21. The common remodeling variant in hypertensive rats. The same variant 2-4c was found in most organs.

We also found two novel variants of remodeling, as predicted. The adrenal TAs exhibited more complex spatial rearrangements. The distal segments with ED ~10-20 μm followed the variant 2-4c, as other organs (**Fig 22A and S9 Fig).** The proximal segments of ED ≈ 30-50 μm transformed oppositely – through the variant 1-6aI with a distended lumen and reduced WTh and

MCSA (**Fig 22B and S10 Fig)**.. This was evident even on 2D graphs (**S6 Fig)**. The adrenals in the 1K1C model experienced a high blood flow. The blood, shunting from clipped or ligated main renal arteries, induced the variant 1-6aI in the proximal segments, i.e. wall distention and thinning, as described for remodeling in high flow models[26],[27],[30]. However, distal TAs demonstrated the same variant 2-4c as in other organs. It may be that smallest arteries (arterioles) are structurally more resistant to distention from high blood flow, due to the absence of elastic laminae and adventitia[100]. Such segmental arterial remodeling has not been verified previously to our knowledge, and indeed was present in TAs with EDs ranging from 10-50 μm.

Fig 22. The distinct remodeling variants in hypertensive rats. (A) Adrenal distal segments of ED ~10-20 μm were congruent with the variant 2-4c, as other organs. Complementary graphs are in **S9 Fig.** (B) Adrenal proximal segments of ED ~30-50 μm were congruent with the variant 1-6aI. Complementary graphs are in **S10 Fig.** (C) The variant 3-4cIII appeared in the kidney. Complementary graphs are in **S11 Fig.**

Renal TAs developed the variant 3-4cIII (**Fig 22C and S11 Fig**), that was responsible for the largest TRR increase. Reduced blood flow in stenotic kidneys[28],[29] should initiate one of the variants (3-4a-b), which has been described for low-flow models[26],[30]. The renal arteries also experienced enhanced RAS activity that likely initiated the variant 2-4c in most organs. Development of the variant 3-4cIII might therefore reflect an interaction between flow-induced and pressure-induced stimuli. We speculated that remodeling by the variant 3-4cIII is a phenomenon of great importance that could be extended beyond the 1K1C model. It is well known that hypertension is combined with atherosclerosis in 70-80% of patients[101]. Therefore

TAs in the brain and heart could be exposed to the low flow due to stenotic atherosclerotic plaques in proximal segments of cerebral and coronary arteries, and activated RAS as well. Presumably, TAs would develop the same variant 3-4cIII with the most increased resistance and reduced flow, which might be responsible for lesions in the heart and brain, being recognized as critical target organs.

We have provided the first quantitative evidence that pulmonary arteries respond to the hypertensive stimulus in 1K1C rats, and in the same remodeling pattern as other organs in the systemic circulation. Our data also represent the first evidence that substantial TAs remodeling occurs in the liver, intestine, and bronchi, which are not considered typical targets in hypertension[5],[25].

The algorithm enables comparison among different studies

Contradictions of two types have been found in conventional remodeling analysis. First, results do not fit the geometric formulae for annular ring dimensions. We applied the term "statistical artifact" (SA) to indicate them. Second, results could be geometrically correct but showed different, opposite, or no remodeling patterns for the same model, organ, or arterial segments (**Table 2, 3 and S3 Table)**. In order to demonstrate that our method could resolve this problem, we used 3D modeling to reanalyze data from studies where linear regression had been calculated, although only few articles could be found. Comparative analysis would not be possible with primary averaged data only.

Two studies claimed unusual non-pressure-related wall thickening after comparing arterial remodeling between aortic coarctation and Goldblatt-induced hypertension in rats[17],[102]. One study[102] demonstrated many SAs (**S5 Table)**. After coarctation, means of WThs and WLRs were elevated despite stable EDs, IDs, and MCSAs. In 1K1C rats, stable IDs

with greater EDs, WThs, and WLRs pointed to the variant 1-5c, although stable MCSAs did not support this designation. A separate study[17] was also inconsistent (**S6 Table).** In both models, averaged dimensions indicated no remodeling in larger segments, but the variant 2-4c in smaller arteries. In coarctation, SA occurred in arteries of ED interval 31-60 μm: unchanged MCSAs did not correspond to stable EDs with lumen narrowing. In two kidney one clip (2K1C) rats, constant EDs and IDs did not follow MCSA and WTh expansion.

Using primary data[17],[102], we calculated linear regressions and applied 3D-modeling. Aortic coarctation exhibited no remodeling in renal or cremaster arteries (**Fig 23A, S12 and S13 Fig),** i.e. there is no non-pressure related TAs thickening distally to aortic coarctation, in normotensive renal and cremaster arteries, as mean values indicated[102],[17]. No further data have been published to support such normotensive thickening[5],[24]. In contrast, the variant 1-6aI has been recognized in the liver[48]. Goldblatt hypertension induced the same variant 2-4c in all segments of cremaster and renal arteries (**Fig 23B and 23C, S14 and S15 Fig**). We also used primary data to recalculate morphometry in renal arteries in SHR[39], and found the variant 2-4c (**Fig 23D and S16 Fig)**.Accordingly, our data suggest that the variant 2-4c is predominant in hypertensive remodeling. The variant 1-5c (stable lumen with wall thickening) was identified in a clinical case of pulmonary hypertension due to congenital mitral stenosis[55] (**Fig 23E and S17 Fig**). That example underlines the precision of our proposed algorithm, since primary data included only fourteen measurements from one pulmonary biopsy. This type of pulmonary hypertension is developed during organogenesis and intensive arterial vascular smooth muscle cells proliferation[103], which could be associated with a stable lumen and wall thickening.

Fig 23. The method enables direct comparison between different studies. (A) Aortic coarctation had no effect on remodeling in renal and cremaster arteries. Complementary graphs are in **S12 and S13 Fig**. (B, C, D) The same variant 2-4c characterized remodeling in cremaster arteries of 1K1C, untouched kidneys of 2K1C rats, and kidneys in SHR respectively. Complementary graphs are in **S14-S16 Fig**. (E) The distinctive variant 1-5c was detected in pulmonary arteries due to congenital mitral valve stenosis Complementary graphs are in **S17**. (F) Data of the subcutaneous arteries was approximated inappropriately with linear regression. Complementary graphs are in **S18 Fig**.

We also tested the linear regression on subcutaneous arteries, reported in patients with essential hypertension[104]. 3D-modeling detected multiple curved lines (**Fig 23F and S18 Fig)** that were the result of an incorrect approximation of the area / length scatterplot by the linear regression. Plotting areas against lengths follows the exponential function[21],[22] (**Fig 19).** The same error we found in other studies[18].

Connecting measurements to hemodynamic values

In addition to proposed TRR and TC, it was also desirable to estimate how media volume had changed in remodeling. The terminal media volume (TMV) could be calculated from complex profiles, similar to TC. However, in the current study we found that variation in accumulated frequencies would significantly affect TC and TMV values. The same negative issue for complex profiles to distinguish remodeling patterns was described above **(Fig 18A**). Accordingly, the linear regression equations, established for each organ, with counting ID and ED for the largest (50 μm) and smallest (10 μm) vessel calibers, provided more reliable estimates. TC and TMV were then computed by the formula for the truncated cone volume:

$$TC = \pi h^{*}(IDlc^{2} + IDlc^{*}\ IDsc + IDsc^{2})\ /3 \qquad (4)$$

$$TMV = \pi h^{*}(EDlc^{2} + EDlc^{*}\ EDsc + EDsc^{2})\ /3 - TC \qquad (5)$$

where EDlc, IDlc and EDsc, IDsc were the largest and smallest caliber limits, respectively, and *h* was the range of calibers (50 μm – 10 μm = 40 μm).

Using this calculation, 1K1C hypertension induced a significant 2 - 5-fold increase in TRR in all organs (**Fig 24A**), correlating significantly with data obtained by physiological measures: in the Goldblatt model increased RVR has been shown in every organ, and is most pronounced in kidneys[105],[106],[107],[108]. It is noteworthy that the kidney has the highest increase in TRR (9-fold), while the pulmonary arteries – the lowest. The increased TRR and TC observed in the adrenal glands were due to different remodeling patterns in the proximal and distal arterial segments.

Fig 24. Hemodynamic parameters are enhanced variously in different organs. (A) There was no clear correlation between the values of TRR, TC, TMV. For example, in the brain enhanced TMV corresponded to a large drop in TC but a small increase in TRR. In the kidney a small elevation in TMV corresponded to a small lowering in TC but augmented TRR. (B) An equal 50% increase in wall expansion in kidney and lung arteries would cause marked differences in TRR and TC increases, while TMV would only increase mildly and remain comparable between the two organs. Different dynamics for TRR, TMV, and TC are the result of different initial organ specific dimensions. x - fold increase.

In normal rats TC correlated with the regional BFR (**Fig 10**). In 1K1C rats TC demonstrated maximum decrease in the brain, liver and intestine, and minimal lowering in the skin, pulmonary

and skeletal muscle arteries **(Fig 24A)**. However, it was difficult to compare our results with pathophysiological studies because regional BFR has been shown as decreased, increased, or stable as well[105],[109],[110]. TMV indicated arterial wall thickening, with maximum of 20-25% in the brain, intestine and pulmonary arteries, and minimum of 2-5% in skeletal muscle, skin and kidney, which were not proportional to TRR and TC (**Fig 24A).** Presumably, basic organ-specific arterial dimensions could have significant impact on hemodynamic consequences of remodeling being the main cause to various organ dynamics of TRR, TC, and TMV (**Fig 24B)**. Evidently, hemodynamic correlations of TRR, TC and TMV need further investigation.

An important goal of our work was to determine if random tissue sections are a reliable source of data. Numerous studies of remodeling, exploring random tissue sections have been published in the past three decades, with most in the 1980s or 1990s, so the majority of our references are dated 15-20 years back. Since then *in vitro* myography studies dominate significantly, while morphometric studies on random sections have been infrequent.

Started from the study[51], the post-mortem contraction has been considered a main cause of high variability in arterial morphometry. Perfusion fixation was intended to eliminate post-mortem arterial contraction, especially with preliminary application of a vasodilator[31] or vessel deactivation[111]. The present study indicates that perfusion fixation is not mandatory for morphometry on random tissue sections. In fact, perfused vs non-perfused organs or myograph experiments demonstrated similar stochastic remodeling patterns (**S3 and S4 Table)**. Here, we avoided fixation deliberately, performing only immersion fixation in order to have animal (and potentially human) material in the same condition for comparison, since for the latter perfusion is unlikely to be applied. Our data prove that careful consideration of arterial tapering is the most

important factor for elaborated morphometry analysis. A similar approach has been widely accepted in atherosclerotic remodeling[93],[57],[112],[113].

In conclusion, we have developed an algorithm to quantify and standardize arterial remodeling analysis. Tissue sampling should be random and representative, according to known recommendations[33],[85]. Following fixation, sections must be stained with periodic acid–Schiff and Masson trichrome. Hematoxylin and eosin staining does not always clearly differentiate muscular and adventitial components, especially when hyalinosis, fibrinoid necrosis, or perivascular inflammatory infiltrates occur[85]. Random measurements of EDs and IDs are performed to obtain about 80-100 measurements of arteries with EDs between ~10-50 µm. Then, variables are arranged in order of increasing ED, divided into 5 µm intervals, and statistical analysis performed for each interval. Finally, the regression equations, complex profiles, remodeling variant, hemodynamic parameters are computed from interval statistics and compared among models or organs. The algorithm does not require additional counting or data gathering, compared to conventional morphometry of arteries on histological sections, and represents a more informative, standardized approach to arterial profiling.

Material and Methods

Experimental protocols were approved by the Animal Ethics Committee at the University of Ottawa and performed according to the recommendations of the Canadian Council for Animal Care. Analyses in normal rats were performed on 20 male Wistar rats (Charles River, Montreal, Québec, Canada), age 20-25 months, and weighing 600-800 g. Five normal male C57BL6 mice (age 20-30 weeks) were used for comparative morphometry. Goldblatt 1K1C hypertension was induced in 20 male Wistar rats (Charles River Laboratories, Montreal, Québec, Canada), age 20-

25 months, weighing 600-800 gm. Under isoflurane anesthesia a silver clip with internal diameter 0.26 mm was placed around the left renal artery and the right kidney was removed. On both sides the manipulation was distal to the adrenal arteries to keep them intact. The control sham-operated group (5 animals) was kept under the same living conditions as the experimental animals. Systolic blood pressure was measured weekly by tail-cuff plethysmography. After 60 days rats were euthanized with an intraperitoneal overdose of sodium pentobarbital. The brain, lung, heart, stomach, liver, small intestine, spleen, kidneys, adrenals, hip skeletal muscle, and tail skin were excised and immersion-fixed in 10% buffered formalin for 24 h, dehydrated and embedded in paraffin. Three fresh lungs from control rats were prepared for special analysis: the entire lobular pulmonary arterial tree was cleaned from parenchyma up to branches of ED 20-30 μm by dissection under a microscope in phosphate-buffered saline. The lung is the only organ which arteries are relatively easy to separate from parenchyma, compare to other organs. Pairs of branches with the same ED but located in proximal and distal segments, 1-2 mm in length were sampled where a branch began, and also embedded in paraffin. Tissue blocks were specifically oriented according to the known anatomical distribution of arteries in order to obtain predominantly cross-circular arterial sections. Histological sections (5 μm thickness) were stained with hematoxylin-eosin and Masson's trichrome. In sections of three to four blocks from each organ, small arteries and arterioles were traced by visual scanning of the entire section. Only vessels with a long- to short-axis ratio < 1.50 were measured. In this way, the error associated with calculating the diameter by averaging the maximum and minimum diameters was minimized (<3%)[33]. The ED and ID were measured in arteries if the profile had a visibly non-interrupted circular or ellipsoid shape. From those two values the derivatives were calculated as follows: WTh = (ED – ID)/2; WLR = WTh /ID; media cross sectional area (MCSA) = π*

842 ($ED^2/2$-$ID^2/2$). Microscopy was performed with a Zeiss AX10microscope (Oberkochen,
843 Germany) and images were analyzed by ImagePro Plus software (Media Cybernetics, Bethesda,
844 MD, USA).

845 Descriptive statistics calculated mean, standard deviation (SD), standard error of mean
846 (SEM), coefficient of variation (CV), and frequency distribution to build histograms and
847 complex profiles. Distribution was assessed by Kolmogorov-Smirnov, D'Agostino & Pearson
848 and Shapiro-Wilk tests. Outliers were identified by the combined robust regression and outlier
849 removal (ROUT) method. Acquired linear regression equations were tested to determine if
850 slopes and intercepts were significantly different ($P < 0.05$) and the goodness of fit coefficient r^2
851 was counted for each equation. Nonlinear regression was approximated with exponential growth
852 equations and the goodness of fit coefficient R^2 was counted for each equation. Extra sum-of-
853 squares F-test and Akaike's Information Criteria (AICc) were used to compare the best-fit values
854 between nonlinear regression equations ($P < 0.05$). Statistical analyses were performed with
855 GraphPad Prism software (GraphPad Software, La Jolla, CA, USA). Modeling procedures were
856 made with MathCAD version 15.0 (Parametric Technology Corporation, Needham, MS, USA).
857 Three-dimensional graphs were built in OriginPro version 2016 SR0 b9.3.226 (OriginLab
858 Corporation, Northampton, MA, USA).

859

860 **Author contributions**

861 Conceived and designed the experiments: AG SA. Performed the experiments: AG SA.
862 Analyzed the data: AG KB PB. Supervision: KB SP. Writing ± review & editing: AG PB KB
863 CK.

References

1. Benjamin EJ, Virani SS, Callaway CW, Chamberlain AM, Chang AR, Cheng S, et al. Heart Disease and Stroke Statistics—2018 Update: A Report From the American Heart Association. Circulation. 2018 Mar 20;137(12):e67–492.
2. Gutsol A, Kashkan A. The graphic analysis of three-dimensional changes of vessels in patients with arterial hypertension. Kardiologiya. 1988;28:48–51.
3. Schiffrin EL, Hayoz D. How to assess vascular remodelling in small and medium-sized muscular arteries in humans. J Hypertens. 1997 Jun;15(6):571–84.
4. Rizzoni D, Agabiti-Rosei E. Structural abnormalities of small resistance arteries in essential hypertension. Intern Emerg Med. 2012 Jun 5;7(3):205–12.
5. Laurent S, Boutouyrie P. The structural factor of hypertension: large and small artery alterations. Circ Res. 2015 Mar 13;116(6):1007–21.
6. Baumbach GL, Heistad DD. Remodeling of cerebral arterioles in chronic hypertension. Hypertension. 1989 Jun;13(6 Pt 2):968–72.
7. Schiffrin EL. Remodeling of resistance arteries in essential hypertension and effects of antihypertensive treatment. Am J Hypertens. 2004 Dec;17(12):1192–200.
8. Cohuet G, Struijker-Boudier H. Mechanisms of target organ damage caused by hypertension: therapeutic potential. Pharmacol Ther. 2006 Jul;111(1):81–98.
9. Kernohan J.W. Keith N.M. AEW. The arterioles in cases of hypertension. Arch Intern Med. 1929;44(3):395–423.
10. Trott DW, Thabet SR, Kirabo A, Saleh MA, Itani H, Norlander AE, et al. Oligoclonal CD8+ T cells play a critical role in the development of hypertension. Hypertens (Dallas, Tex 1979). 2014 Nov;64(5):1108–15.
11. Mulvany MJ, Baumbach GL, Aalkjaer C, Heagerty AM, Korsgaard N, Schiffrin EL, et al.

888 Vascular remodeling. Hypertension. 1996 Sep;28(3):505–6.

889 12. Nordborg C, Ivarsson H, Johansson BB, Stage L. Morphometric study of mesenteric and
890 renal arteries in spontaneously hypertensive rats. J Hypertens. 1983 Dec;1(4):333–8.

891 13. Kinuno H, Tomoda F, Koike T, Takata M, Inoue H. Effects of uninephrectomy on renal
892 structural properties in spontaneously hypertensive rats. Clin Exp Pharmacol Physiol.
893 2005 Mar;32(3):173–8.

894 14. Leh S, Hultström M, Rosenberger C, Iversen BM. Afferent arteriolopathy and glomerular
895 collapse but not segmental sclerosis induce tubular atrophy in old spontaneously
896 hypertensive rats. Virchows Arch. 2011 Jul;459(1):99–108.

897 15. Ohara M, Tomoda F, Koike T, Liu H, Uno K, Nitta A, et al. Pubertal administration of
898 antiserum against nerve growth factor regresses renal vascular remodeling in
899 spontaneously hypertensive rats. Clin Exp Pharmacol Physiol. 2015 Jun;42(6):687–94.

900 16. Smeda JS, Lee RM, Forrest JB. Structural and reactivity alterations of the renal
901 vasculature of spontaneously hypertensive rats prior to and during established
902 hypertension. Circ Res. 1988 Sep;63(3):518–33.

903 17. Liu JL, Bishop SP, Overbeck HW. Morphometric evidence for non-pressure-related
904 arterial wall thickening in hypertension. Circ Res. 1988 May;62(5):1001–10.

905 18. Owens GK, Schwartz SM, McCanna M. Evaluation of medial hypertrophy in resistance
906 vessels of spontaneously hypertensive rats. Hypertension. 1988 Feb;11(2):198–207.

907 19. Casare FAM, Thieme K, Costa-Pessoa JM, Rossoni LV, Couto GK, Fernandes FB, et al.
908 Renovascular remodeling and renal injury after extended angiotensin II infusion. Am J
909 Physiol - Ren Physiol. 2016 Jun 1;310(11):F1295–307.

910 20. De Ciuceis C, Amiri F, Brassard P, Endemann DH, Touyz RM, Schiffrin EL. Reduced

911 vascular remodeling, endothelial dysfunction, and oxidative stress in resistance arteries of
912 angiotensin II-infused macrophage colony-stimulating factor-deficient mice: evidence for
913 a role in inflammation in angiotensin-induced vascular injury. Arterioscler Thromb Vasc
914 Biol. 2005 Oct 1;25(10):2106–13.
915 21. Berry CL, Henrichs KJ. Morphometric investigation of hypertrophy in the arteries of
916 DOCA-hypertensive rats. J Pathol. 1982 Feb;136(2):85–94.
917 22. Ashen MD, Hamlyn JM. Smooth muscle hypertrophy and arterial remodelling in
918 deoxycorticosterone acetate-salt hypertension. Clin Exp Hypertens. 1994 May;16(3):261–
919 82.
920 23. London GM, Marchais SJ, Guerin AP, Metivier F, Adda H. Arterial structure and function
921 in end-stage renal disease. Nephrol Dial Transplant. 2002 Oct;17(10):1713–24.
922 24. Heagerty AM, Heerkens EH, Izzard AS. Small artery structure and function in
923 hypertension. J Cell Mol Med. 2010 May;14(5):1037–43.
924 25. Lee RM, Dickhout JG, Sandow SL. Vascular structural and functional changes: their
925 association with causality in hypertension: models, remodeling and relevance. Hypertens
926 Res. 2017 Apr 27;40(4):311–23.
927 26. Wesselman JPM, Kuijs R, Hermans JJR, Janssen GMJ, Fazzi GE, van Essen H, et al. Role
928 of the Rhoa/Rho Kinase System in Flow-Related Remodeling of Rat Mesenteric Small
929 Arteries in Vivo. J Vasc Res. 2004 Jun 30;41(3):277–90.
930 27. Bouvet C, de Chantemele EB, Guihot A-L, Vessieres E, Bocquet A, Dumont O, et al.
931 Flow-Induced Remodeling in Resistance Arteries From Obese Zucker Rats Is Associated
932 With Endothelial Dysfunction. Hypertension. 2007 Jul 1;50(1):248–54.
933 28. Chade AR, Zhu X, Lavi R, Krier JD, Pislaru S, Simari RD, et al. Endothelial Progenitor

Cells Restore Renal Function in Chronic Experimental Renovascular Disease. Circulation. 2009 Jan 19;119(4):547–57.

29. Favreau F, Zhu X-Y, Krier JD, Lin J, Warner L, Textor SC, et al. Revascularization of swine renal artery stenosis improves renal function but not the changes in vascular structure. Kidney Int. 2010 Dec;78(11):1110–8.

30. Ceiler DL, De Mey JG. Chronic N(G)-nitro-L-arginine methyl ester treatment does not prevent flow-induced remodeling in mesenteric feed arteries and arcading arterioles. Arterioscler Thromb Vasc Biol. 2000 Sep;20(9):2057–63.

31. Bund SJ, Lee RMKW. Arterial structural changes in hypertension: a consideration of methodology, terminology and functional consequence. J Vasc Res. 2003;40(6):547–57.

32. Lee RM, Smeda JS. Primary versus secondary structural changes of the blood vessels in hypertension. Can J Physiol Pharmacol. 1985 Apr;63(4):392–401.

33. Weibel ER. Stereological Methods: Theoretical Foundations. Vol. 2. Academic Press; 1980. 340 p.

34. Dao HH, Martens FM, Larivière R, Yamaguchi N, Cernacek P, de Champlain J, et al. Transient involvement of endothelin in hypertrophic remodeling of small arteries. J Hypertens. 2001 Oct;19(10):1801–12.

35. New DI, Chesser AM, Thuraisingham RC, Yaqoob MM. Structural remodeling of resistance arteries in uremic hypertension. In: Kidney International. 2004. p. 1818–25.

36. Whitworth JA, Hewitson TD, Ming L, Wilson RS, Scoggins BA, Wright RD, et al. Adrenocorticotrophin-induced hypertension in the rat: haemodynamic, metabolic and morphological characteristics. J Hypertens. 1990 Jan;8(1):27–36.

37. Liu DT, Birchall I, Hewitson T, Kincaid-Smith P, Whitworth JA. Effect of dietary calcium

on the development of hypertension and hypertensive vascular lesions in DOCA-salt and two-kidney, one clip hypertensive rats. J Hypertens. 1994 Feb;12(2):145–53.

38. Lü L, Yao T, Zhu Y-Z, Huang G-Y, Cao Y-X, Zhu Y-C. Chronic all-trans retinoic acid treatment prevents medial thickening of intramyocardial and intrarenal arteries in spontaneously hypertensive rats. Am J Physiol Heart Circ Physiol. 2003 Oct;285(4):H1370-7.

39. Racasan S, Hahnel B, Van Der Giezen DM, Blezer EL, Goldschmeding R, Braam B, et al. Temporary losartan or captopril in young SHR induces malignant hypertension despite initial normotension. Kidney Int. 2004;65(2):575–81.

40. Mazzali M, Kanellis J, Han L, Feng L, Xia YY, Chen Q, et al. Hyperuricemia induces a primary renal arteriolopathy in rats by a blood pressure-independent mechanism. Am J Physiol Ren Physiol. 2002;282(6):F991-7.

41. Sánchez-Lozada LG, Tapia E, Santamaría J, Avila-Casado C, Soto V, Nepomuceno T, et al. Mild hyperuricemia induces vasoconstriction and maintains glomerular hypertension in normal and remnant kidney rats. Kidney Int. 2005;67(1):237–47.

42. Tapia E, Franco M, Sánchez-Lozada LG, Soto V, Avila-Casado C, Santamaría J, et al. Mycophenolate mofetil prevents arteriolopathy and renal injury in subtotal ablation despite persistent hypertension. Kidney Int. 2003 Mar;63(3):994–1002.

43. Kang D-H, Nakagawa T, Feng L, Johnson RJ. Nitric oxide modulates vascular disease in the remnant kidney model. Am J Pathol. 2002 Jul;161(1):239–48.

44. Helmchen U, Kneissler U, Bohle RM, Reher A, Groene HJ. Adaptation and decompensation of intrarenal small arteries in experimental hypertension. J Cardiovasc Pharmacol. 1984;6 Suppl 4:S696-705.

980 45. Polichnowski AJ, Cowley AW. Pressure-induced renal injury in angiotensin II versus
981 norepinephrine-induced hypertensive rats. Hypertension. 2009 Dec;54(6):1269–77.
982 46. Zar J. Biostatistical analysis. 5th ed. Upper Saddle River, NJ,USA: Prentice-Hall; 2010.
983 944 p.
984 47. Lee RM, Forrest JB, Garfield RE, Daniel EE. Comparison of blood vessel wall
985 dimensions in normotensive hypertensive rats by histometric and morphometric methods.
986 Blood Vessels. 1983;20(5):245–54.
987 48. Novikov Y V, Shormanov S V, Kulikov S V. Reversibility of changes in hepatic vessels
988 after correction of experimental aortic coarctation. Bull Exp Biol Med. 2006
989 Apr;141(4):479–82.
990 49. Briones AM, Xavier FE, Arribas SM, González MC, Rossoni L V, Alonso MJ, et al.
991 Alterations in structure and mechanics of resistance arteries from ouabain-induced
992 hypertensive rats. Am J Physiol Heart Circ Physiol. 2006 Jul 24;291(1):H193-201.
993 50. Limas C, Westrum B, Limas CJ. The evolution of vascular changes in the spontaneously
994 hypertensive rat. Am J Pathol. 1980 Feb;98(2):357–84.
995 51. Furuyama M. Histometrical investigations of arteries in reference to arterial hypertension.
996 Tohoku J Exp Med. 1962 May 25;76:388–414.
997 52. van Heijst A, Haasdijk R, Groenman F, van der Staak F, Hulsbergen-van de Kaa C, de
998 Krijger R, et al. Morphometric analysis of the lung vasculature after extracorporeal
999 membrane oxygenation treatment for pulmonary hypertension in newborns. Virchows
1000 Arch. 2004 Jul 3;445(1):36–44.
1001 53. Hislop A, Reid L. Normal structure and dimensions of the pulmonary arteries in the rat. J
1002 Anat. 1978 Jan;125(Pt 1):71–83.

1003 54. Short DS, Thomson AD. The arteries of the small intestine in systemic hypertension. J
1004 Pathol Bacteriol. 1959 Oct;78:321–34.
1005 55. Yamaki S, Endo M, Takahashi T. Different grades of medial hypertrophy and intimal
1006 changes in small pulmonary arteries among various types of congenital heart disease with
1007 pulmonary hypertension. Tohoku J Exp Med. 1997;182(1):83–91.
1008 56. Jing L, Zhang J, Sun J, Guo F, An X, Yang K, et al. Inhibition of extracellular signal-
1009 regulated kinases ameliorates hypertension-induced renal vascular remodeling in rat
1010 models. Int J Mol Sci. 2011 Nov 28;12(12):8333–46.
1011 57. Gutierrez J, Goldman J, Honig LS, Elkind MSV, Morgello S, Marshall RS. Determinants
1012 of cerebrovascular remodeling: Do large brain arteries accommodate stenosis?
1013 Atherosclerosis. 2014 Aug;235(2):371–9.
1014 58. Korshunov VA, Daul M, Massett MP, Berk BC. Axl mediates vascular remodeling
1015 induced by deoxycorticosterone acetate-salt hypertension. Hypertension.
1016 2007;50(6):1057–62.
1017 59. Kett MM, Alcorn D, Bertram JF, Anderson WP. Enalapril does not prevent renal arterial
1018 hypertrophy in spontaneously hypertensive rats. Hypertension. 1995 Mar;25(3):335–42.
1019 60. Simon G, Jäckel M, Illyes G. Role of angiotensin II, sympathetic stimulation and salt in
1020 the development of structural vascular changes in rat kidney. Clin Exp Pharmacol Physiol.
1021 2003 Jul;30(7):476–81.
1022 61. Nordborg C, Johansson B. Morphometric study on cerebral vessels in spontaneously
1023 hypertensive rats. Stroke. 1980;11:266–70.
1024 62. Baumbach GL, Sigmund CD, Bottiglieri T, Lentz SR. Structure of cerebral arterioles in
1025 cystathionine beta-synthase-deficient mice. Circ Res. 2002 Nov 15;91(10):931–7.

1026 63. Hanstede JG, Gerrits PO. Caliber and media thickness of intrahepatic arteries in a normal
1027 human liver. A morphometric study. Acta Morphol Neerl Scand. 1986;24(4):281–92.
1028 64. Imhof E. Cartographic relief presentation. Redlands, CA, USA: ESRI Press; 2007. 436 p.
1029 65. Davis JC. Statistics and Data Analysis in Geology. Sons JW&, editor. New York, NY:
1030 Wiley; 2002. 635 p.
1031 66. Tekin E, Hunt D, Newberry MG, Savage VM. Do Vascular Networks Branch Optimally
1032 or Randomly across Spatial Scales? Mac Gabhann F, editor. PLOS Comput Biol. 2016
1033 Nov 30;12(11):e1005223.
1034 67. Brekke JF, Gokina NI, Osol G. Vascular smooth muscle cell stress as a determinant of
1035 cerebral artery myogenic tone. Am J Physiol Heart Circ Physiol. 2002 Dec;283(6):H2210-
1036 6.
1037 68. Denton KM, Anderson WP, Sinniah R. Effects of angiotensin II on regional afferent and
1038 efferent arteriole dimensions and the glomerular pole. Am J Physiol Regul Integr Comp
1039 Physiol. 2000 Aug;279(2):R629–38.
1040 69. Shweta A, Denton KM, Kett MM, Bertram JF, Lambert GW, Anderson WP. Paradoxical
1041 structural effects in the unilaterally denervated spontaneously hypertensive rat kidney. J
1042 Hypertens. 2005 Apr;23(4):851–9.
1043 70. Kuwahira I, Gonzalez NC, Heisler N, Piiper J. Changes in regional blood flow distribution
1044 and oxygen supply during hypoxia in conscious rats. J Appl Physiol. 1993;74(1):211–4.
1045 71. Greenblatt EP, Loeb AL, Longnecker DE. Marked regional heterogeneity in the
1046 magnitude of EDRF/NO-mediated vascular tone in awake rats. J Cardiovasc Pharmacol.
1047 1993 Feb;21(2):235–40.
1048 72. MacLean MR, Hiley CR. Effect of neuropeptide Y on cardiac output, its distribution,

regional blood flow and organ vascular resistances in the pithed rat. Br J Pharmacol. 1990 Feb;99(2):340–2.

73. Sakaeda T, Fukumura K, Takahashi K, Matsumura S, Matsuura E, Hirano K. Blood flow rate in normal and tumor-bearing rats in conscious state, under urethane anesthesia, and during systemic hypothermia. J Drug Target. 1998;6(4):261–72.

74. Boswell CA, Mundo EE, Ulufatu S, Bumbaca D, Cahaya HS, Majidy N, et al. Comparative physiology of mice and rats: radiometric measurement of vascular parameters in rodent tissues. Mol Pharm. 2014 May 5;11(5):1591–8.

75. Neves MF, Virdis A, Schiffrin EL. Resistance artery mechanics and composition in angiotensin II-infused rats: effects of aldosterone antagonism. J Hypertens. 2003 Jan;21(1):189–98.

76. Skogstrand T, Leh S, Paliege A, Reed RK, Vikse BE, Bachmann S, et al. Arterial damage precedes the development of interstitial damage in the nonclipped kidney of two-kidney, one-clip hypertensive rats. J Hypertens. 2013 Jan;31(1):152–9.

77. Deng LY, Schiffrin EL. Morphological and functional alterations of mesenteric small resistance arteries in early renal hypertension in rats. Am J Physiol. 1991 Oct;261(4 Pt 2):H1171-7.

78. Tsamis A, Stergiopulos N. Arterial remodeling in response to hypertension using a constituent-based model. Am J Physiol Heart Circ Physiol. 2007 Nov;293(5):H3130-9.

79. Sadd M. Elasticity: Theory, Applications, and Numerics. 3rd ed. Waltham, MA USA: Elsevier Inc; 2014. 582 p.

80. Gasser TC, Ogden RW, Holzapfel GA. Hyperelastic modelling of arterial layers with distributed collagen fibre orientations. J R Soc Interface. 2006 Feb 22;3(6):15–35.

1072 81. Rizzoni D, Rodella L, Porteri E, Rezzani R, Guelfi D, Piccoli A, et al. Time course of
1073 apoptosis in small resistance arteries of spontaneously hypertensive rats. J Hypertens.
1074 2000 Jul;18(7):885–91.
1075 82. Qin X-P, Zeng S-Y, Tian H-H, Deng S-X, Ren J-F, Zheng Y-B, et al. Involvement of
1076 prolylcarboxypeptidase in the effect of rutaecarpine on the regression of mesenteric artery
1077 hypertrophy in renovascular hypertensive rats. Clin Exp Pharmacol Physiol. 2009
1078 Mar;36(3):319–24.
1079 83. Zeng J, Huang R, Su Z. Stroke-prone renovascular hypertensive rats. Chin Med J (Engl).
1080 1998 Aug;111(8):741–4.
1081 84. Hill GS, Heudes D, Jacquot C, Gauthier E, Bariéty J. Morphometric evidence for
1082 impairment of renal autoregulation in advanced essential hypertension. Kidney Int. 2006
1083 Mar;69(5):823–31.
1084 85. Schoen FJ. Robbins Basic Pathology. In: Kumar V, Abbas A FN, editor. Pathologic Basis
1085 of Disease. 7th ed. Philadelphia: Elsevier Saunders; 2012. p. 511–54.
1086 86. Ceron CS, Rizzi E, Guimaraes DA, Martins-Oliveira A, Cau SB, Ramos J, et al. Time
1087 course involvement of matrix metalloproteinases in the vascular alterations of
1088 renovascular hypertension. Matrix Biol. 2012 May;31(4):261–70.
1089 87. Zhou N, Wang T, Song J, He H, He J, He L. Antihypertensive and vascular remodelling
1090 effects of the imperatorin derivative OW1 in renovascular hypertension rats. Clin Exp
1091 Pharmacol Physiol. 2014 Aug;41(8):571–8.
1092 88. VAN CITTERS RL, WAGNER BM, RUSHMER RF. Architecture of small arteries
1093 during vasoconstriction. Circ Res. 1962 Apr;10:668–75.
1094 89. DeCiuceis C, Porteri E, Rizzoni D, Rizzardi N, Paiardi S, Boari G, et al. Structural

Alterations of Subcutaneous Small-Resistance Arteries May Predict Major Cardiovascular Events in Patients With Hypertension. Am J Hypertens. 2007 Aug;20(8):846–52.

90. Korsgaard N, Mulvany MJ. Cellular hypertrophy in mesenteric resistance vessels from renal hypertensive rats. Hypertens (Dallas, Tex 1979). 1988 Aug;12(2):162–7.

91. Johansson BB. Cerebral vascular bed in hypertension and consequences for the brain. Hypertension. 1984;6(6 Pt 2):III81-6.

92. Kost CK, Herzer WA, Li P, Notoya M, Mizuhira V, Inagami T, et al. Angiotensin II-induced structural and functional alterations in spontaneously hypertensive rat kidney. Am J Physiol. 1996 Jan;270(1 Pt 2):F229-36.

93. Glagov S, Weisenberg E, Zarins CK, Stankunavicius R, Kolettis GJ. Compensatory Enlargement of Human Atherosclerotic Coronary Arteries. N Engl J Med. 1987 May 28;316(22):1371–5.

94. Bhui R, Hayenga HN. An agent-based model of leukocyte transendothelial migration during atherogenesis. Marsden A, editor. PLoS Comput Biol. 2017 May 25;13(5):e1005523.

95. Gabeler EEE, van Hillegersberg R, Statius van Eps RG, Sluiter W, Gussenhoven EJ, Mulder P, et al. A comparison of balloon injury models of endovascular lesions in rat arteries. BMC Cardiovasc Disord. 2002 Sep 27;2:16.

96. Nordborg C, Petursdottir V. Vessel wall morphometry in giant cell arteritis. Arthritis Care Res. 2000 Oct;13(5):286–90.

97. Montaudon M, Berger P, Lederlin M, Marthan R, Tunon-de-Lara JM, Laurent F. Bronchial morphometry in smokers: comparison with healthy subjects by using 3D CT. Eur Radiol. 2009 Jun 24;19(6):1328–34.

1118 98. Heagerty AM, Aalkjaer C, Bund SJ, Korsgaard N, Mulvany MJ. Small artery structure in
1119 hypertension. Dual processes of remodeling and growth. Hypertension. 1993
1120 Apr;21(4):391–7.
1121 99. Swokowski EW, Cole JA. Algebra and trigonometry with analytic geometry. 13rd editi.
1122 Cengage Learning. Cengage Learning; 2012. 960 p.
1123 100. Chobanian A V, Prescott MF, Haudenschild CC. Recent advances in molecular pathology.
1124 The effects of hypertension on the arterial wall. Exp Mol Pathol. 1984 Aug;41(1):153–69.
1125 101. Herrington W, Lacey B, Sherliker P, Armitage J, Lewington S. Epidemiology of
1126 Atherosclerosis and the Potential to Reduce the Global Burden of Atherothrombotic
1127 Disease. Circ Res. 2016 Feb 19;118(4):535–46.
1128 102. Plunkett WC, Overbeck HW. Increased arteriolar wall-to-lumen ratio in a normotensive
1129 vascular bed in coarctation hypertension. Am J Physiol. 1985 Oct;249(4 Pt 2):H859-66.
1130 103. Fediuk J, Gutsol A, Nolette N, Dakshinamurti S. Thromboxane-induced actin
1131 polymerization in hypoxic pulmonary artery is independent of Rho. AJP Lung Cell Mol
1132 Physiol. 2012 Jan 1;302(1):L13–26.
1133 104. Izzard AS, Rizzoni D, Agabiti-Rosei E, Heagerty AM. Small artery structure and
1134 hypertension: adaptive changes and target organ damage. J Hypertens. 2005
1135 Feb;23(2):247–50.
1136 105. van Boom M, Saxena PR. Systemic and regional haemodynamics in experimental renal
1137 hypertension in conscious rabbits. Clin Exp Pharmacol Physiol. 1980 Nov;7(6):627–34.
1138 106. Teranishi Y, Iriuchijima J. Regional blood flows and resistances in conscious one-kidney,
1139 one-clip renovascular hypertensive rats. Jpn J Physiol. 1988;38(1):47–53.
1140 107. Boegehold MA, Huffman LJ, Hedge GA. Peripheral vascular resistance and regional

blood flows in hypertensive Dahl rats. Am J Physiol. 1991 Oct;261(4 Pt 2):R934-8.

108. Anderson WP, Shweta A, Evans RG, Edgley AJ, Gao Y. Total peripheral resistance responsiveness during the development of secondary renal hypertension in dogs. J Hypertens. 2007 Mar;25(3):649–62.

109. Charocopos F, Hatzinikolaou P, Gavras I, Gavras H. Regional blood flows and cardiac hemodynamics in renovascular and mineralocorticoid hypertensive rats. J Physiol (Paris). 1984;79(3):162–5.

110. Liard JF. Regional blood flows in running normotensive and renal hypertensive dogs. J Hypertens. 1986 Aug;4(4):399–406.

111. Baumbach GL, Didion SP, Faraci FM. Hypertrophy of Cerebral Arterioles in Mice Deficient in Expression of the Gene for CuZn Superoxide Dismutase. Stroke. 2006 Jul 1;37(7):1850–5.

112. Gutierrez J, Elkind MS V, Virmani R, Goldman J, Honig L, Morgello S, et al. A pathological perspective on the natural history of cerebral atherosclerosis. Int J Stroke. 2015 Oct 8;10(7):1074–80.

113. Qiao Y, Anwar Z, Intrapiromkul J, Liu L, Zeiler SR, Leigh R, et al. Patterns and Implications of Intracranial Arterial Remodeling in Stroke Patients. Stroke. 2016 Feb;47(2):434–40.

Supporting information captions

S1 Table. Normality tests for averaged arterial dimensions in the kidney, heart and pulmonary arteries.

S1 Fig. Complex profiles revealed different tapering patterns in organs. Complementary

graphs to **Fig 6A.** Axis X – the bidirectional common linear scale for the external diameter (ED), wall thickness (WTh), and internal diameter (ID); axis Y – accumulated frequency of variables (%).

S2 Fig. Linear regression equations and RR in different organs. Lines and RR (blue curves) represent the best fit for different organs. Complementary graphs to **Fig 6B.** Points are mean ± SD for 5-μm ED intervals; r^2 - goodness of fit coefficients. Corresponding equations are in **S2 Table.**

S2 Table. Linear regression equations from mean ± SD for 5 μm ED intervals.

S3 Fig. Comparison of linear regressions for ID and WTh between different organs. Equations for lungs, bronchi, adrenal glands, stomach and skeletal muscles were very distinctive ($P<0.0001$). Brain and intestine (*) shared similar equations ($P>0.41$ for ID and WTh). Heart and spleen (**) were also close ($P>0.43$ for ID and >0.83 for WTh). Equations for kidney, liver and skin (***) were similar ($P>0.77$ for ID and >0.87 for WTh).

S4 Fig. Histograms of terminal arteries in the kidney, heart and brain. The significant irregularity and asymmetry for dimensions used to calculate statistics in **Table 2.** Data did not pass conventional statistical tests for normality (negative, $P<0.001$).

S3 Table. Numerical classification applied to arteries studied via in vitro myography. 1K1C, one kidney-one clip; 2K1C, two kidney-one clip; Ang, angiotensin; DM2, diabetes mellitus type 2; EHT, essential hypertension; eNOS, endothelial nitric oxide synthase; GI, growth index; L-NAME, Nitro-L-arginine methyl ester; op/+, osteopetrotic heterozygous; PM, pressure myograph; RI, remodeling index; RVH, renovascular hypertension; SA, statistical artifact; SHR, spontaneously hypertensive rats; SHRSP, spontaneously hypertensive rats stroke prone; SOD, superoxide dismutase; WM, wire myograph.

S4 Table. Linear regression equations of terminal arteries derived from mean ± SD for 5-µm ED intervals. All equations for hypertensive rats were significantly different from equations for control rats ($r^2 = 0.99$; $P < 0.0001$).

S5 Fig. Control vs hypertensive complex profiles in organs. Control (green) and hypertensive (red) complex profiles were superimposed. Remodeling patterns are not recognizable. Complementary graphs to **Fig 18A.**

S6 Fig. Linear regression lines displaced similarly in most organs. The ID slopes decreased (solid arrows), and the WTh slopes increased (dashed arrows). Adrenal arteries demonstrated opposite directions: the increased ID slopes and decreased WTh slopes. Complementary graphs to **Fig 18B.**

S7 Fig. The remodeling of renal arteries has been simulated for variants 2-4c, 2-6a, all 3-4, 3-5a, and 3-6a. Displacement of linear regression lines up or down for any parameter was similar for many remodeling variants. Complementary graphs to **Fig 19.**

S8 Fig. 3D-modeling simulation for the brain. No variants were congruent. Complementary graphs to **Figure 20.**

S9 Fig. 3D-modeling simulation for the distal arterial segments in the adrenals. No variants, except 2-4c, were congruent. Complementary graphs to **Fig 22A**.

S10 Fig. 3D-modeling simulation for the proximal arterial segments in the adrenals. If the variant 1-6aI appeared, congruence to the variant 2-6a must also be present because data sets overlap. Complementary graphs to **Fig 22B.**

S11 Fig. 3D-modeling simulation for the kidney. If the variant 3-4cIII occurred, simultaneous congruence to 2-4c and 3-4cII (but not 3-4cI) must be present because data sets overlap. Complementary graphs to **Fig 22C**.

S5 Table. Averaged arterial dimensions in rats with aortic coarctation and 1K1C hypertension (modified from[102]). NC, numerical classification; SA – statistical artifact; ↑ indicates increase in dimensions vs sham values, *P<0.05, ** P<0.01.

S6 Table. Averaged arterial dimensions in rats with aortic coarctation and 2K1C hypertension (modified from[17]). 2K1C, two-kidney, one clip; NC, numerical classification; SA – statistical artifact; ↑ ↓ indicates increase or decrease in dimensions vs sham values, *P<0.05, ** P<0.01, *** P<0.001

S12 Fig. Cremaster arteries in normotensive rats with aortic coarctation have no remodeling. The control and experimental equations were not different (the variant 2-5b; P > 0.6-0.7). Calculated from[102]. Complementary graphs to **Fig 23A.**

S13 Fig. Renal interlobular arteries in normotensive rats with aortic coarctation have no remodeling. The control and experimental equations were not different (the variant 2-5b; P > 0.8). Calculated from[17]. Complementary graphs to **Fig 23A.**

S14 Fig. Cremaster arteries in hypertensive 1K1C rats developed the variant 2-4c. Calculated from[102]. Complementary graphs to **Fig 23B.**

S15 Fig. Renal arteries in 2K1C rats were congruent to the variant 2-4c. Calculated from[17]. Complementary graphs to **Fig 23C.**

S16 Fig. Renal arteries in SHR showed congruence to the variant 2-4c. Calculated from[39]. Complementary graphs to **Fig 23D.**

S17 Fig. Pulmonary arteries in a case of pulmonary hypertension due to congenital mitral stenosis developed the variant 1-5c. Calculated from[55]. Complementary graphs to **Fig 23E.**

S18 Fig. Recalculated data from human subcutaneous arteries[104]**.** The graph length vs area has been approximated with the linear regression, resulting in curved lines. Complementary

graphs to **Fig 23F.**

S19 Video. 3-D modeling for the brain. The video demonstrates the variant 2-4c as congruent.

S20 Video. 3-D modeling for the brain. The video demonstrates the variant 3-4aIII as an example of a non-congruent variant.

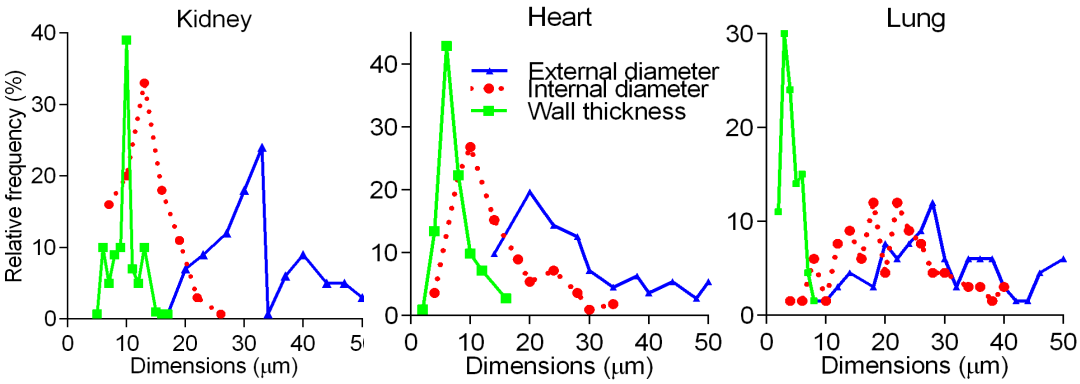
Kidney
Heart
Lung
External diameter
Internal diameter
Wall thickness
Relative frequency (%)
Dimensions (μm)

Fig 1.

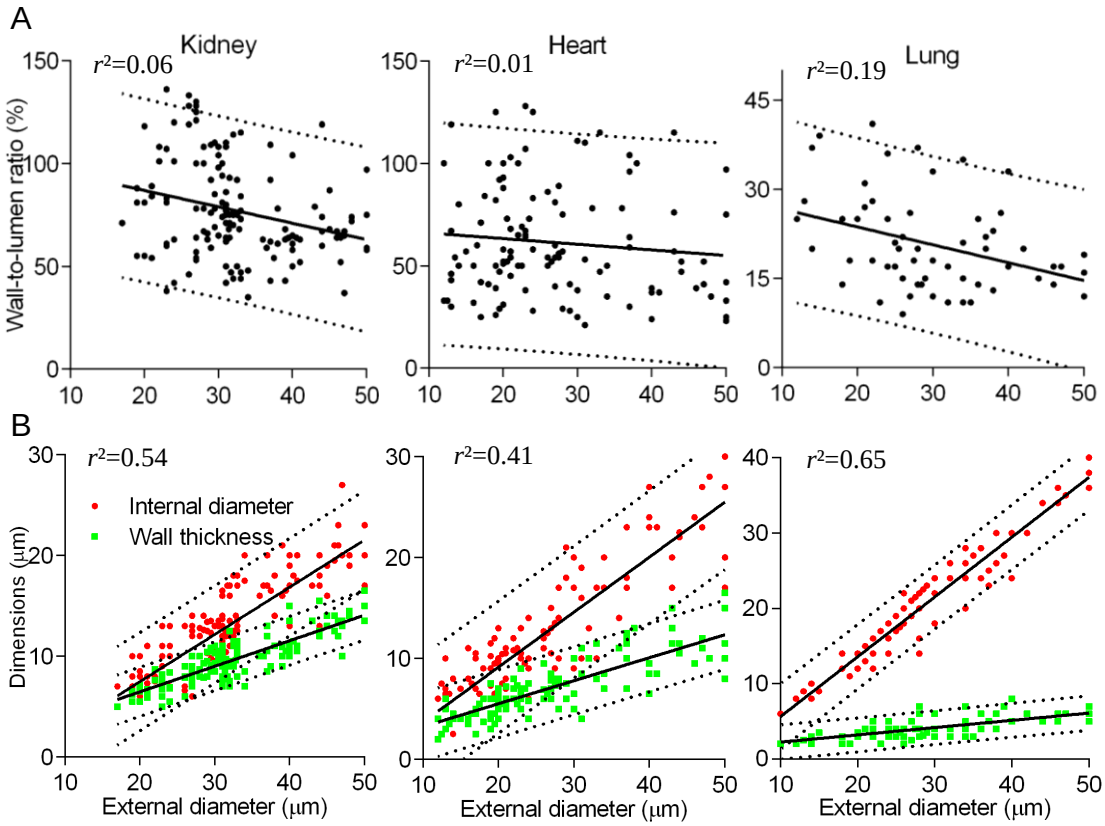
A
Kidney
Heart
Lung
r²=0.06
r²=0.01
r²=0.19
Wall-to-lumen ratio (%)
B
r²=0.54
r²=0.41
r²=0.65
Internal diameter
Wall thickness
Dimensions (μm)
External diameter (μm)

Fig 2.

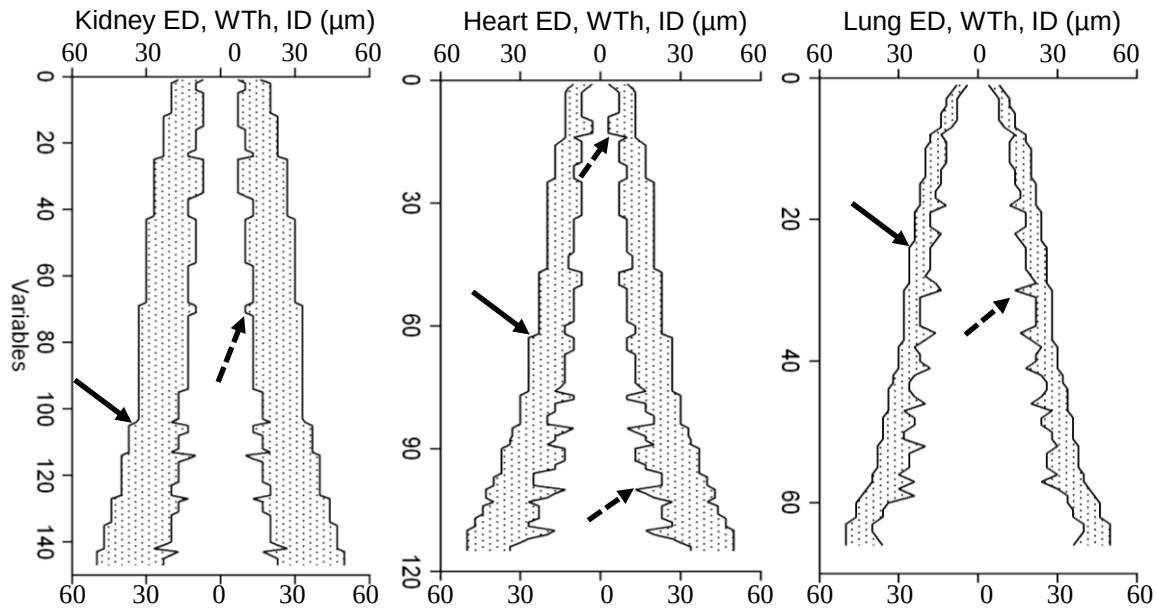
Kidney ED, WTh, ID (µm)
Heart ED, WTh, ID (µm)
Lung ED, WTh, ID (µm)
Variables

Fig 3.

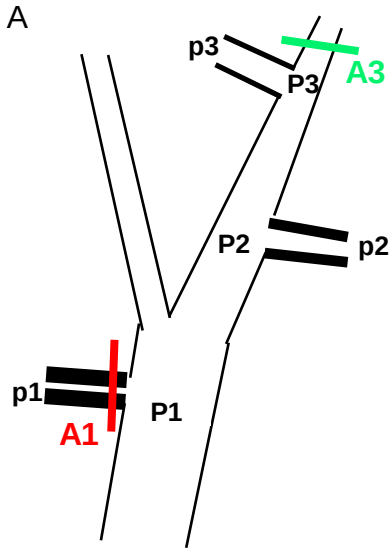

C

Branch type	ED µm	ID µm	WTh µm	WLR %
Proximal, axillary or sympodial	28	14	7	50
Distal, regular dichotomous	28	22	3	14
Proximal, axillary or sympodial	32	12	10	83
Distal, regular dichotomous	32	26	3	12
Proximal, axillary or sympodial	38	20	9	45
Distal, regular dichotomous	38	30	4	13
Proximal, axillary or sympodial	40	22	9	41
Distal, regular dichotomous	40	34	3	9
Proximal, axillary or sympodial	44	22	10	45
Distal, regular dichotomous	44	34	5	15

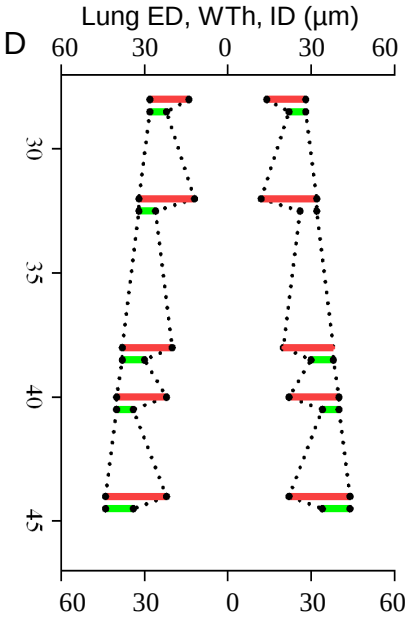

Fig 4.

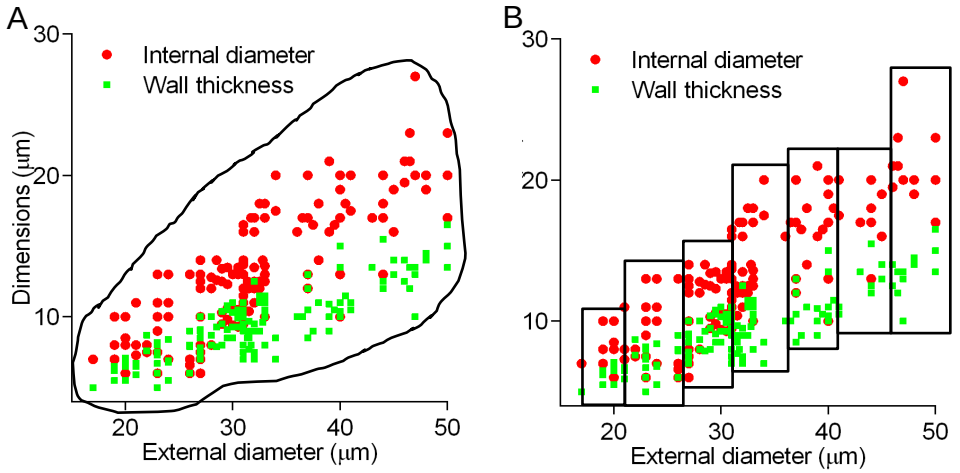
A
B
Internal diameter
Wall thickness
Dimensions (μm)
External diameter (μm)

Fig 5.

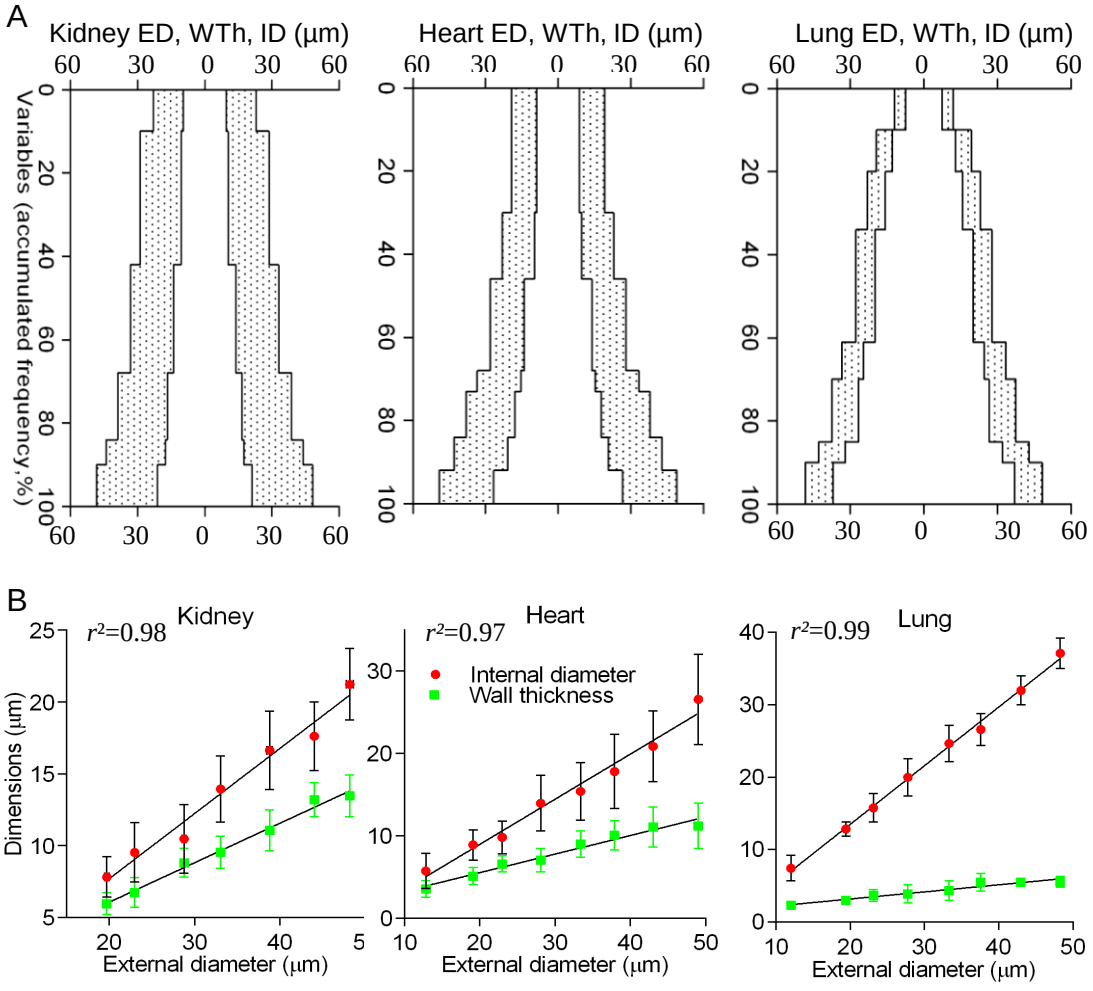
A
Kidney ED, WTh, ID (μm)
Heart ED, WTh, ID (μm)
Lung ED, WTh, ID (μm)
Variables (accumulated frequency,%)
B
Kidney
Heart
Lung
r²=0.98
r²=0.97
r²=0.99
Internal diameter
Wall thickness
Dimensions (μm)
External diameter (μm)

Fig 6.

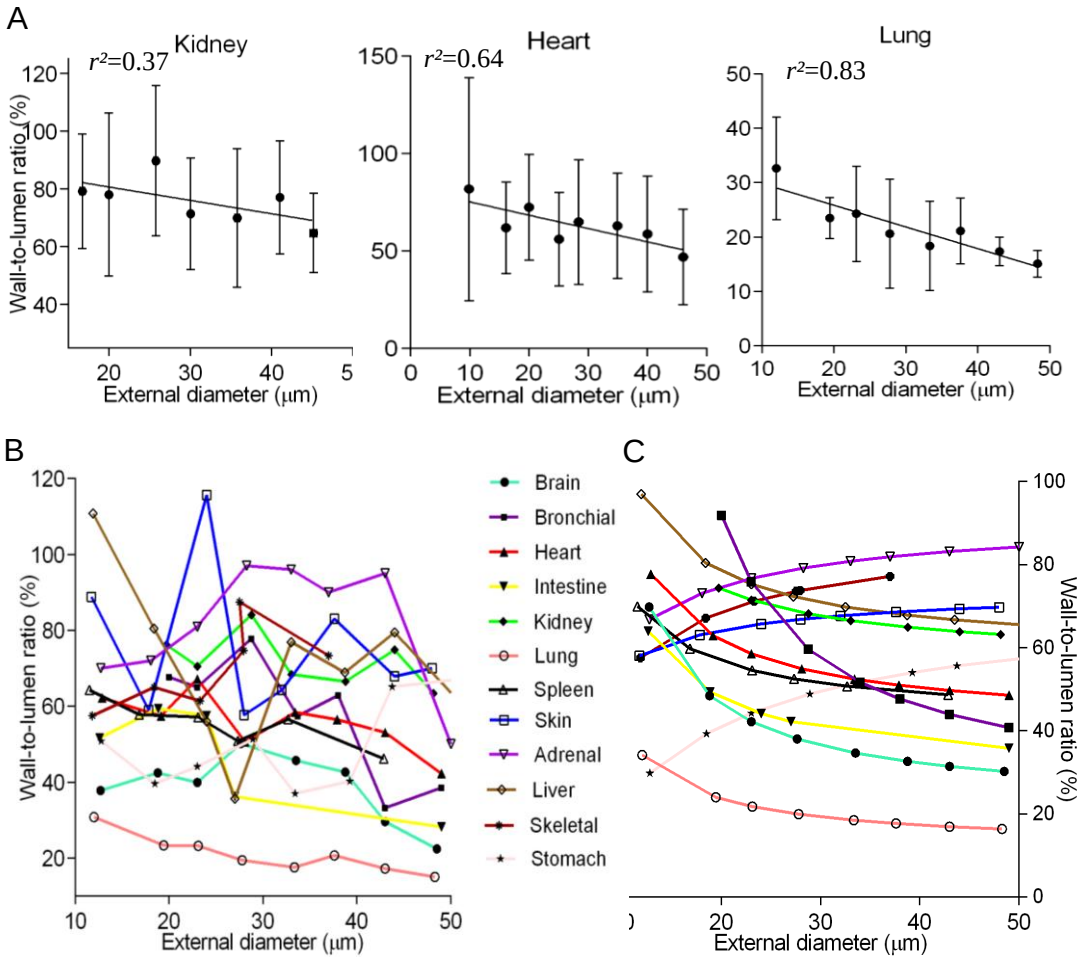
A
Kidney
r^2=0.37
Heart
r^2=0.64
Lung
r^2=0.83
Wall-to-lumen ratio (%)
External diameter (μm)
B
Wall-to-lumen ratio (%)
External diameter (μm)
Brain
Bronchial
Heart
Intestine
Kidney
Lung
Spleen
Skin
Adrenal
Liver
Skeletal
Stomach
C
Wall-to-lumen ratio (%)
External diameter (μm)

Fig 7.

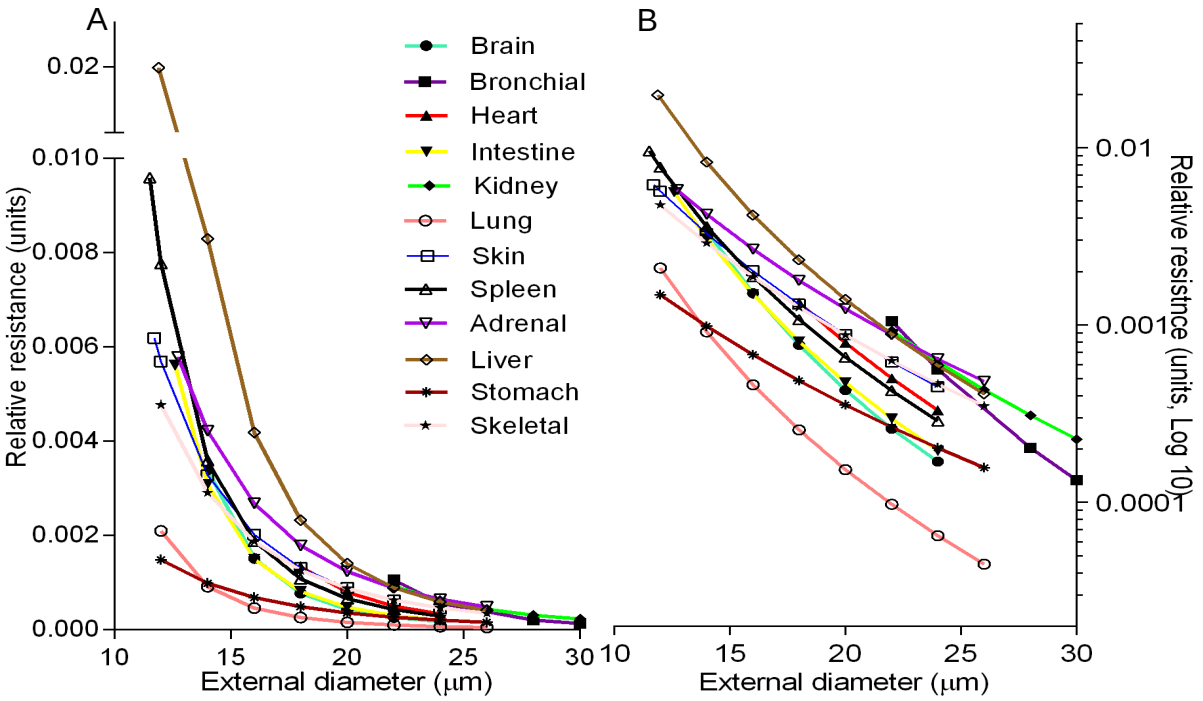
A
B
Brain
Bronchial
Heart
Intestine
Kidney
Lung
Skin
Spleen
Adrenal
Liver
Stomach
Skeletal
Relative resistance (units)
Relative resistnce (units, Log 10)
External diameter (μm)
External diameter (μm)
0.02
0.010
0.008
0.006
0.004
0.002
0.000
0.01
0.001
0.0001
10
15
20
25
30

Fig 8.

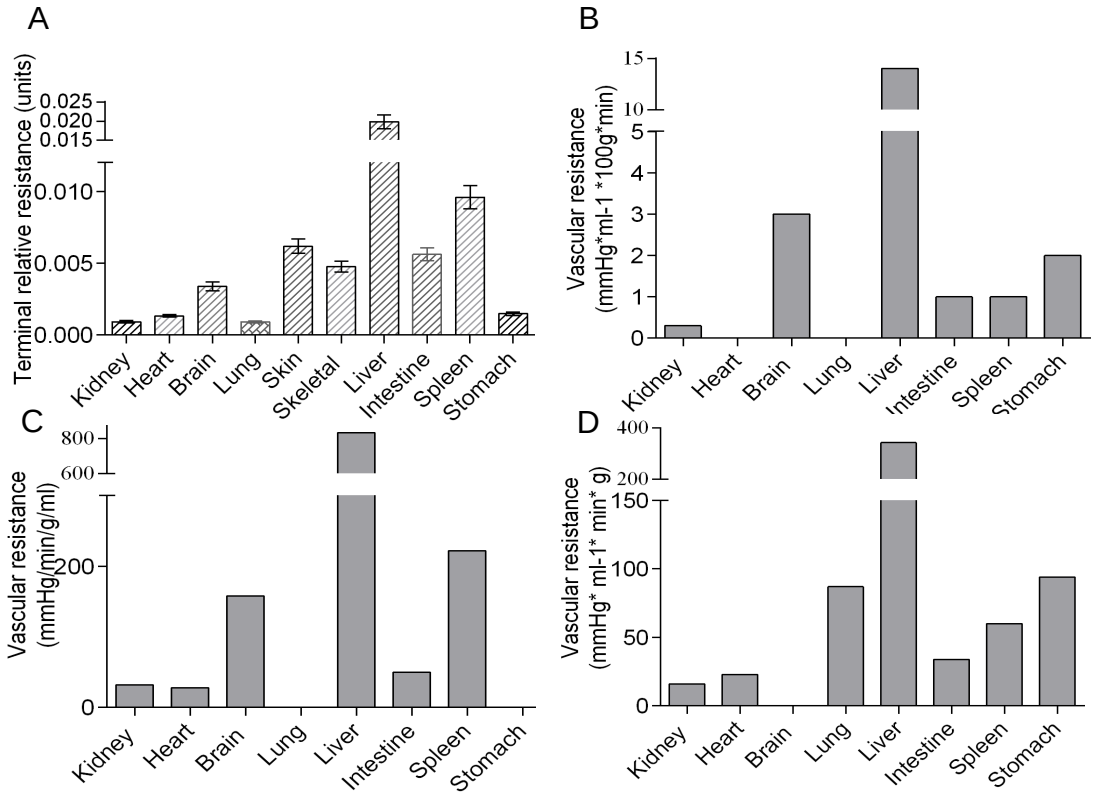
A
Terminal relative resistance (units)
0.025
0.020
0.015
0.010
0.005
0.000
Kidney
Heart
Brain
Lung
Skin
Skeletal
Liver
Intestine
Spleen
Stomach
B
Vascular resistance
(mmHg*ml-1 *100g*min)
15
10
5
4
3
2
1
0
Kidney
Heart
Brain
Lung
Liver
Intestine
Spleen
Stomach
C
Vascular resistance
(mmHg/min/g/ml)
800
600
200
0
Kidney
Heart
Brain
Lung
Liver
Intestine
Spleen
Stomach
D
Vascular resistance
(mmHg* ml-1* min* g)
400
200
150
100
50
0
Kidney
Heart
Brain
Lung
Liver
Intestine
Spleen
Stomach

Fig 9.

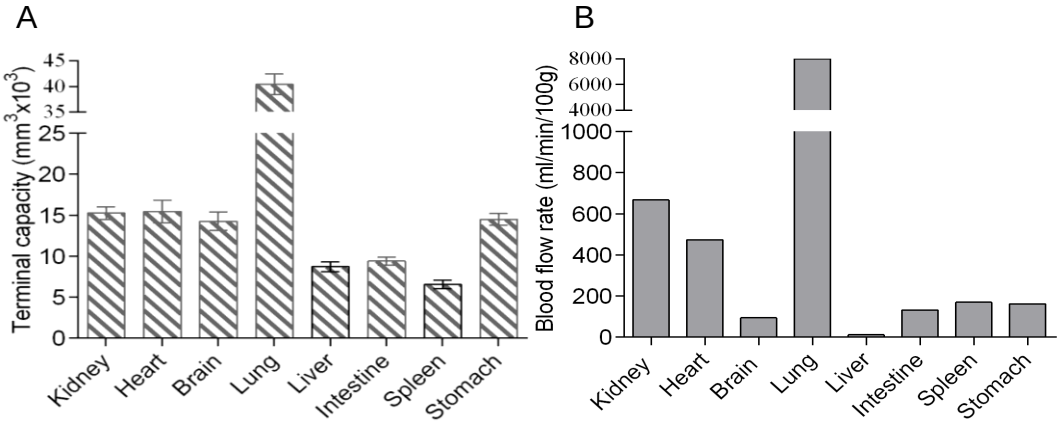
A
Terminal capacity (mm3x10-3)
45
40
35
25
20
15
10
5
0
Kidney
Heart
Brain
Lung
Liver
Intestine
Spleen
Stomach
B
Blood flow rate (ml/min/100g)
8000
6000
4000
1000
800
600
400
200
0
Kidney
Heart
Brain
Lung
Liver
Intestine
Spleen
Stomach

Fig 10.

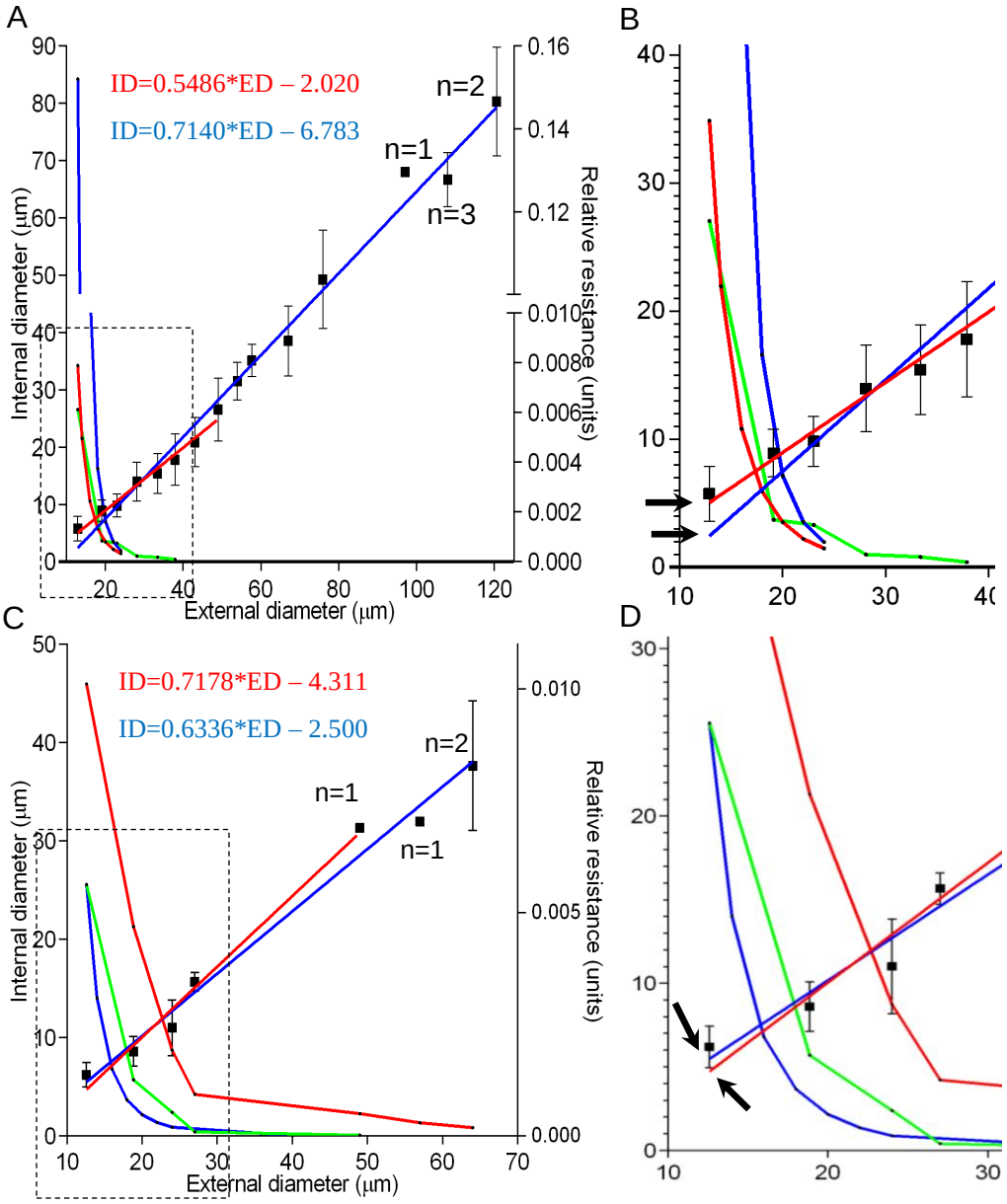
A
ID=0.5486*ED – 2.020
ID=0.7140*ED – 6.783
n=2
n=1
n=3
Internal diameter (μm)
Relative resistance (units)
External diameter (μm)
B
C
ID=0.7178*ED – 4.311
ID=0.6336*ED – 2.500
n=2
n=1
n=1
Internal diameter (μm)
Relative resistance (units)
External diameter (μm)
D

Fig 11.

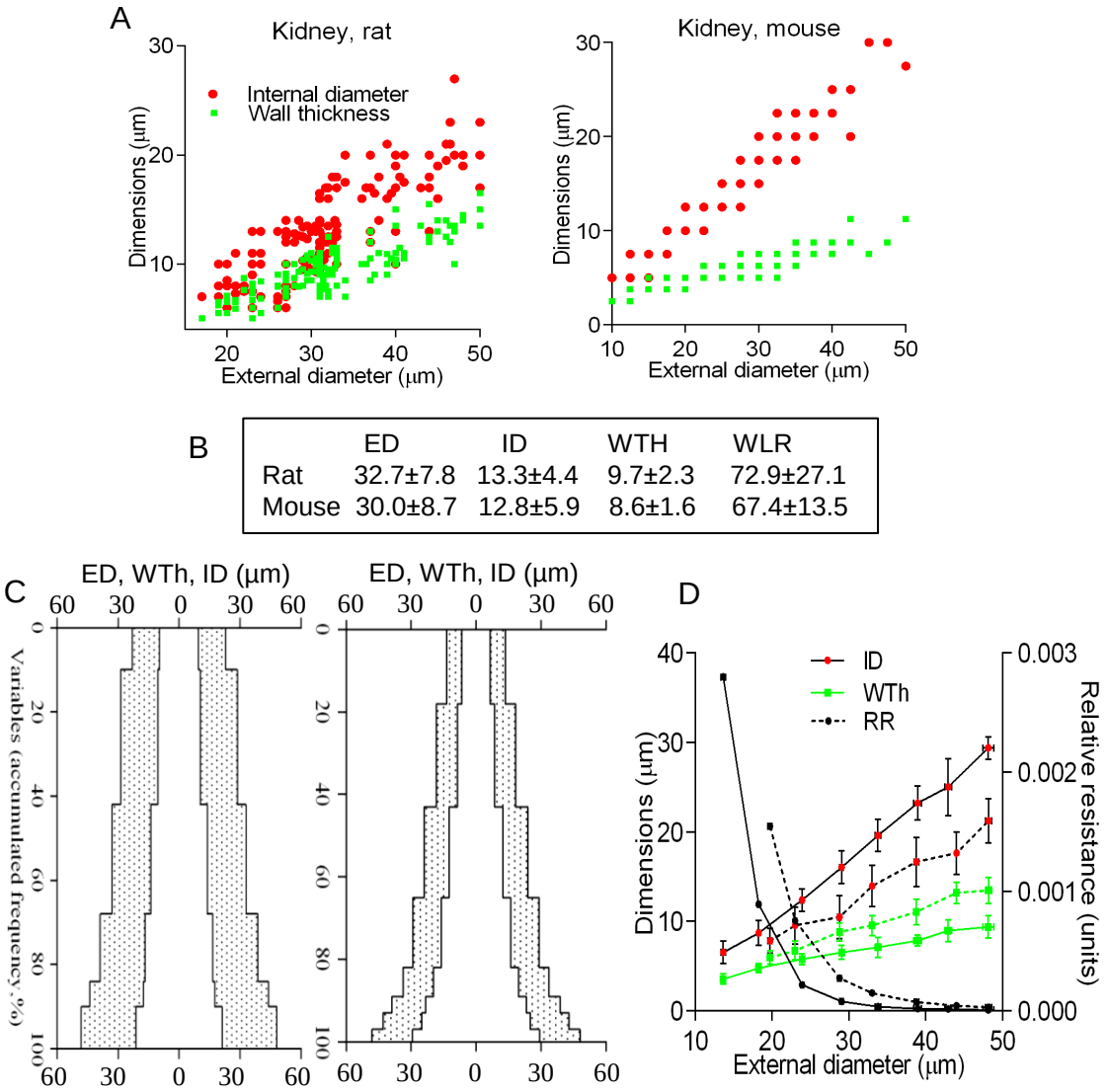

	ED	ID	WTH	WLR
Rat	32.7±7.8	13.3±4.4	9.7±2.3	72.9±27.1
Mouse	30.0±8.7	12.8±5.9	8.6±1.6	67.4±13.5

Fig 12.

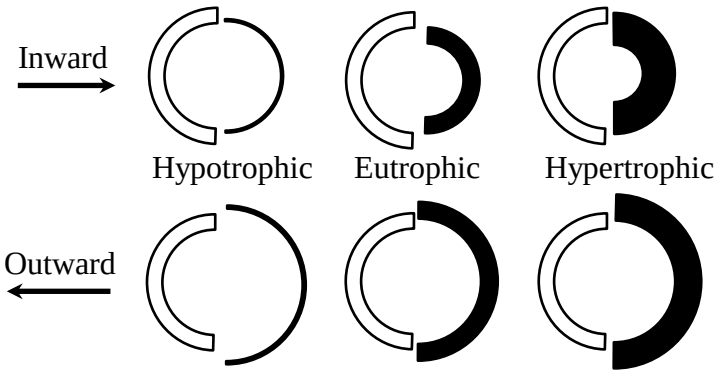
Inward
Hypotrophic
Eutrophic
Hypertrophic
Outward

Fig 13.

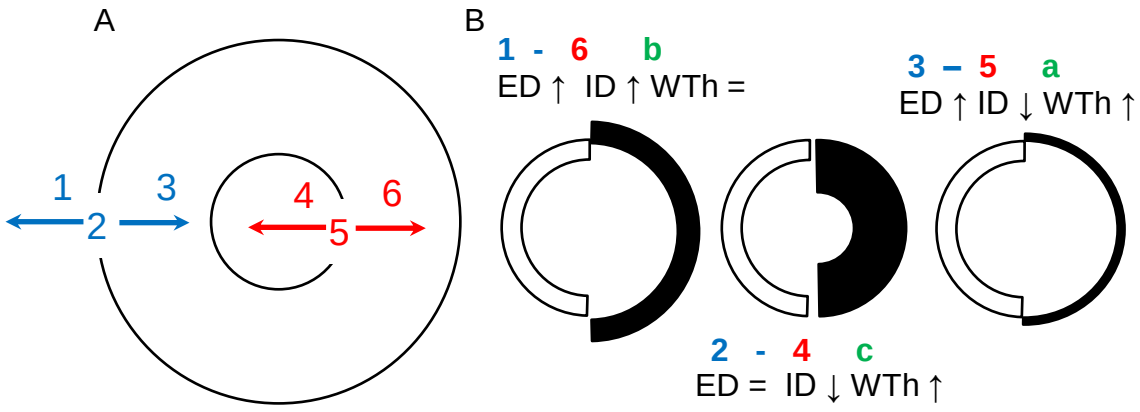
A
1
2
3
4
5
6
B
1 - 6 b
ED ↑ ID ↑ WTh =
3 – 5 a
ED ↑ ID ↓ WTh ↑
2 - 4 c
ED = ID ↓ WTh ↑

Fig 14.

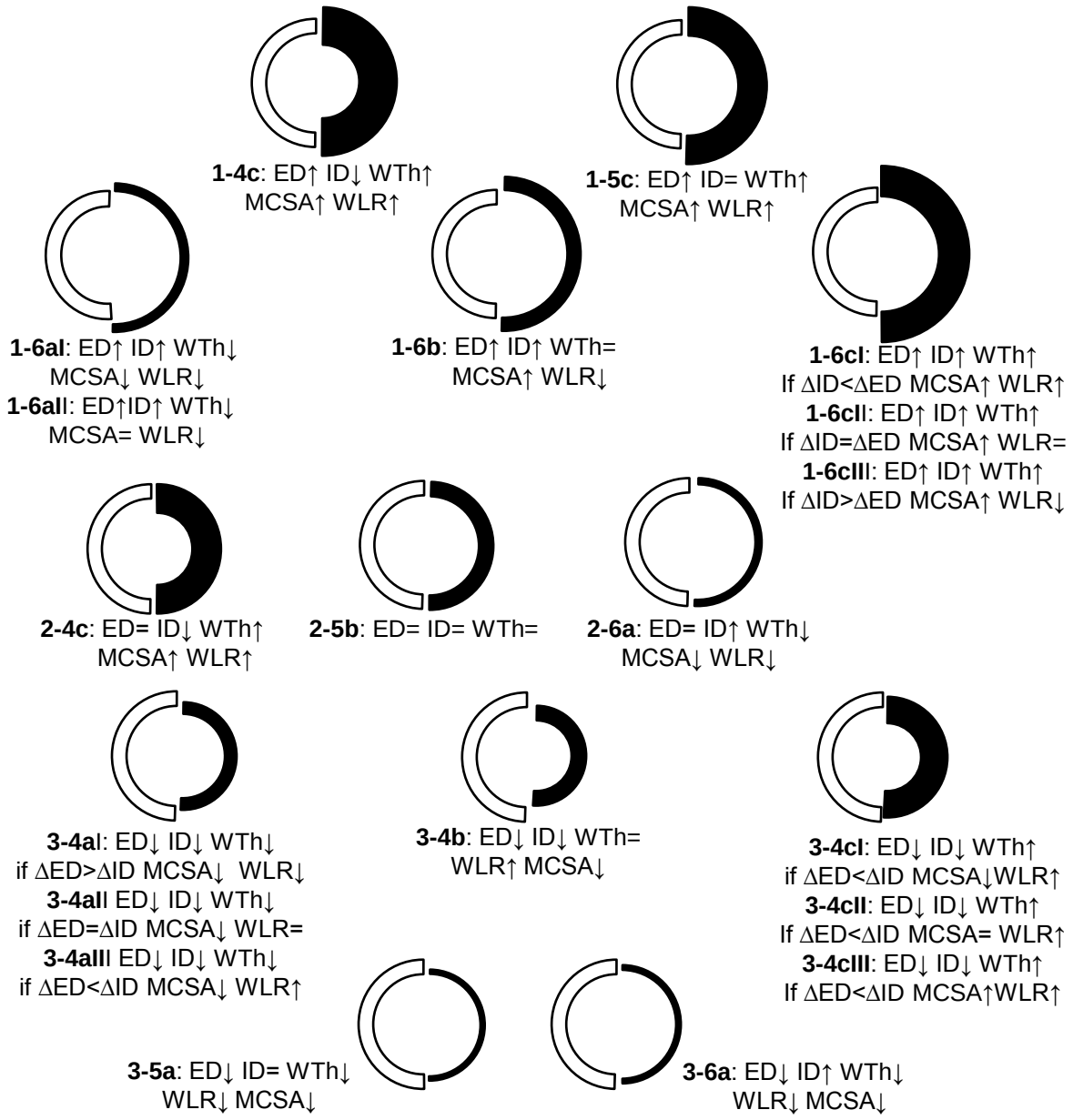
1-4c: ED↑ ID↓ WTh↑
MCSA↑ WLR↑
1-5c: ED↑ ID= WTh↑
MCSA↑ WLR↑
1-6aI: ED↑ ID↑ WTh↓
MCSA↓ WLR↓
1-6aII: ED↑ID↑ WTh↓
MCSA= WLR↓
1-6b: ED↑ ID↑ WTh=
MCSA↑ WLR↓
1-6cI: ED↑ ID↑ WTh↑
If ΔID<ΔED MCSA↑ WLR↑
1-6cII: ED↑ ID↑ WTh↑
If ΔID=ΔED MCSA↑ WLR=
1-6cIII: ED↑ ID↑ WTh↑
If ΔID>ΔED MCSA↑ WLR↓
2-4c: ED= ID↓ WTh↑
MCSA↑ WLR↑
2-5b: ED= ID= WTh=
2-6a: ED= ID↑ WTh↓
MCSA↓ WLR↓
3-4aI: ED↓ ID↓ WTh↓
if ΔED>ΔID MCSA↓ WLR↓
3-4aII ED↓ ID↓ WTh↓
if ΔED=ΔID MCSA↓ WLR=
3-4aIII ED↓ ID↓ WTh↓
if ΔED<ΔID MCSA↓ WLR↑
3-4b: ED↓ ID↓ WTh=
WLR↑ MCSA↓
3-4cI: ED↓ ID↓ WTh↑
if ΔED<ΔID MCSA↓WLR↑
3-4cII: ED↓ ID↓ WTh↑
If ΔED<ΔID MCSA= WLR↑
3-4cIII: ED↓ ID↓ WTh↑
If ΔED<ΔID MCSA↑WLR↑
3-5a: ED↓ ID= WTh↓
WLR↓ MCSA↓
3-6a: ED↓ ID↑ WTh↓
WLR↓ MCSA↓

Fig 15.

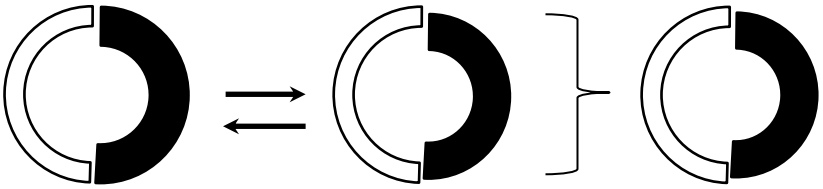

2-4c: ED↔ ID↓ WTh↑ MCSA↑ WLR↑

3-4cII: ED↓ ID↓ WTh↑ If ΔED<ΔID MCSA= WLR↑

3-4cIII: ED↓ ID↓ WTh↑ If ΔED<ΔID MCSA↑WLR↑

Fig 16.

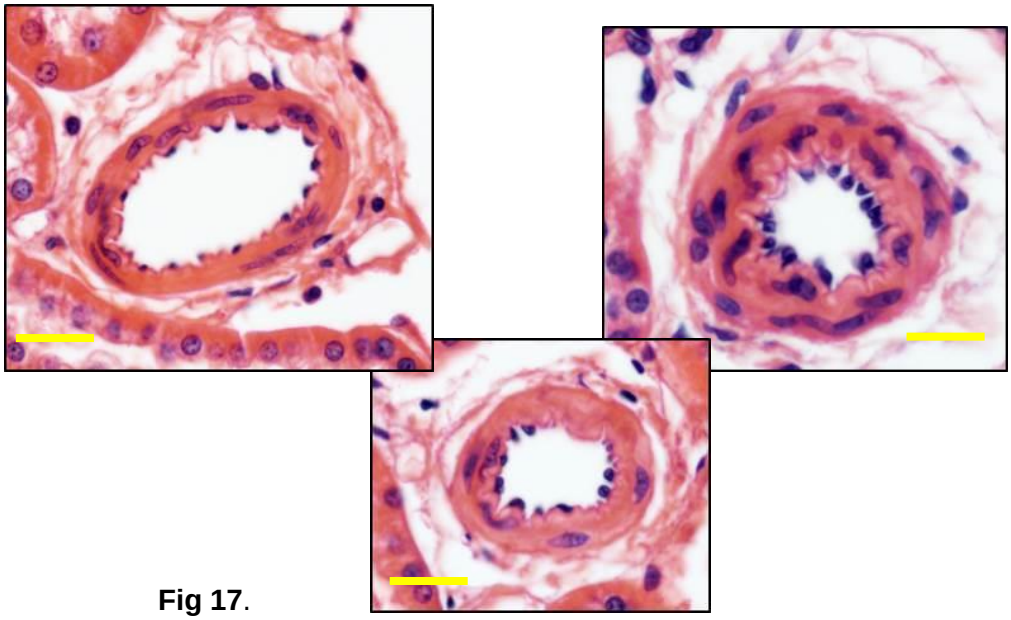

Fig 17.

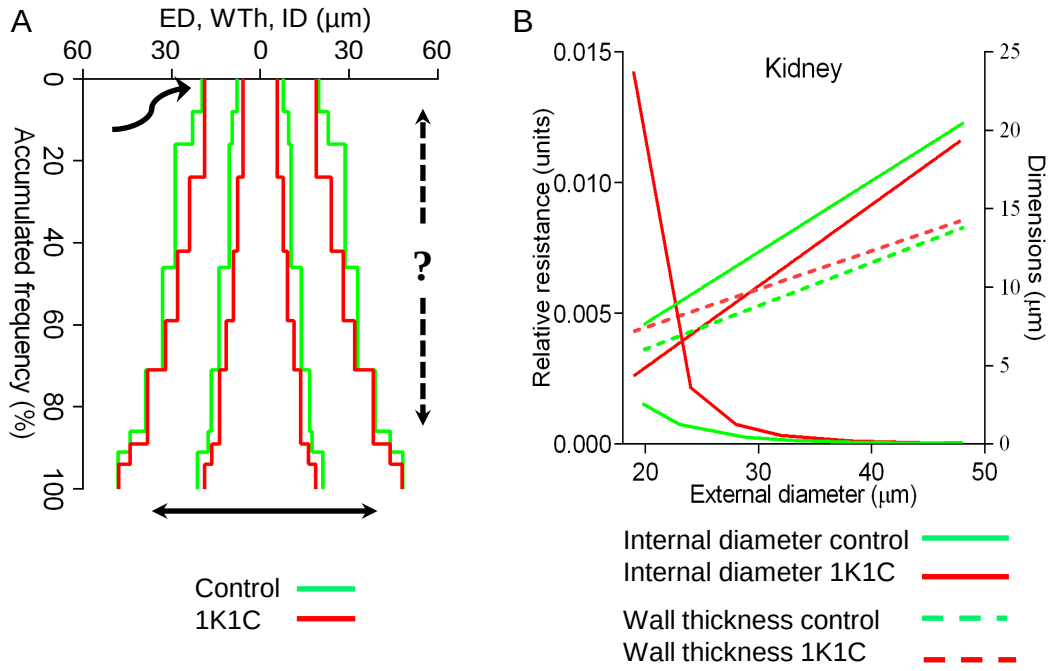
A
ED, WTh, ID (µm)
60
30
0
30
60
0
20
40
60
80
100
Accumulated frequency (%)
?
Control
1K1C
B
Kidney
0.015
0.010
0.005
0.000
Relative resistance (units)
25
20
15
10
5
0
Dimensions (µm)
20
30
40
50
External diameter (µm)
Internal diameter control
Internal diameter 1K1C
Wall thickness control
Wall thickness 1K1C

Fig 18.

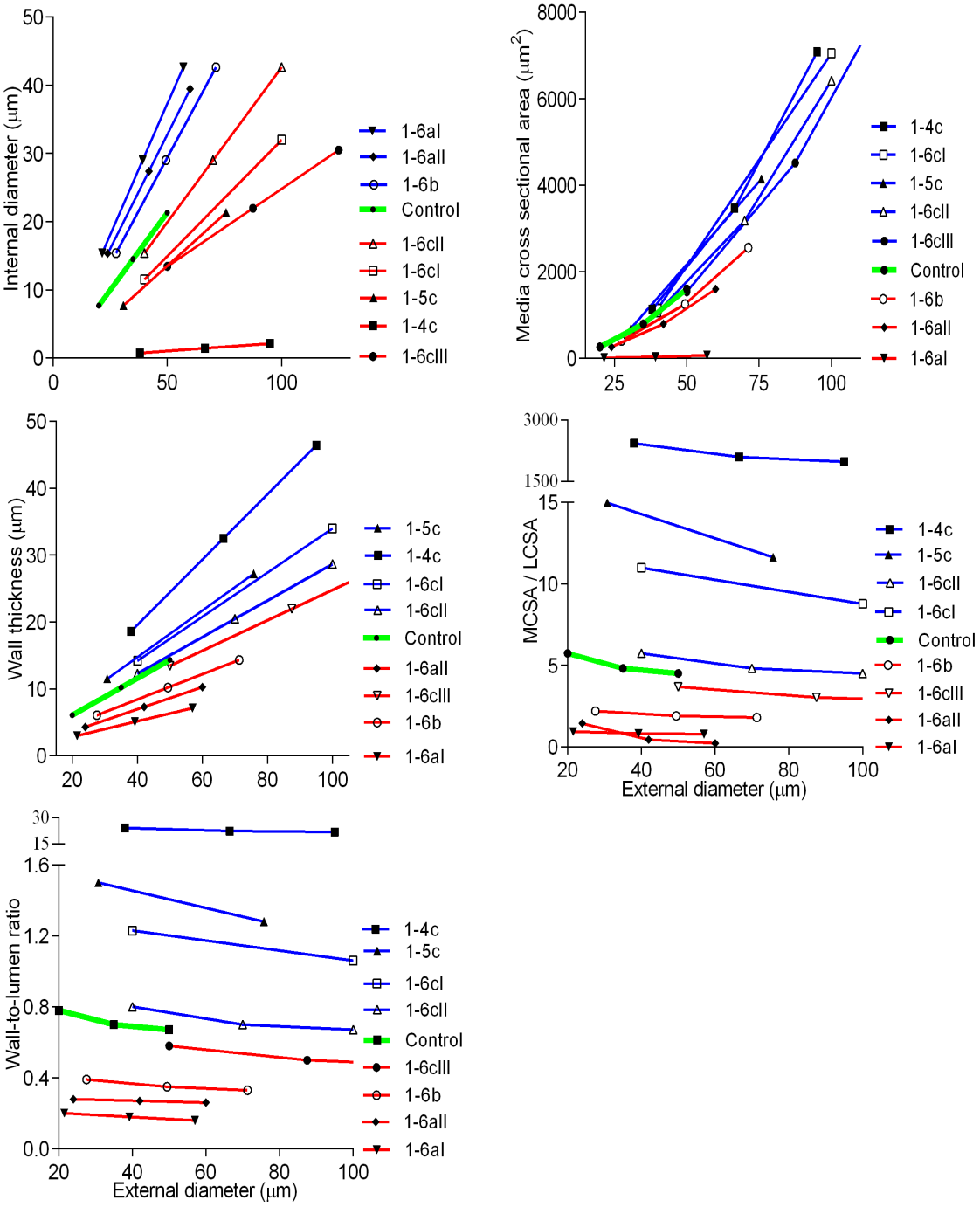
Internal diameter (μm)
1-6aI
1-6aII
1-6b
Control
1-6cII
1-6cI
1-5c
1-4c
1-6cIII
Media cross sectional area (μm²)
1-4c
1-6cI
1-5c
1-6cII
1-6cIII
Control
1-6b
1-6aII
1-6aI
Wall thickness (μm)
1-5c
1-4c
1-6cI
1-6cII
Control
1-6aII
1-6cIII
1-6b
1-6aI
MCSA / LCSA
External diameter (μm)
1-4c
1-5c
1-6cII
1-6cI
Control
1-6b
1-6cIII
1-6aII
1-6aI
Wall-to-lumen ratio
External diameter (μm)
1-4c
1-5c
1-6cI
1-6cII
Control
1-6cIII
1-6b
1-6aII
1-6aI

Fig 19.

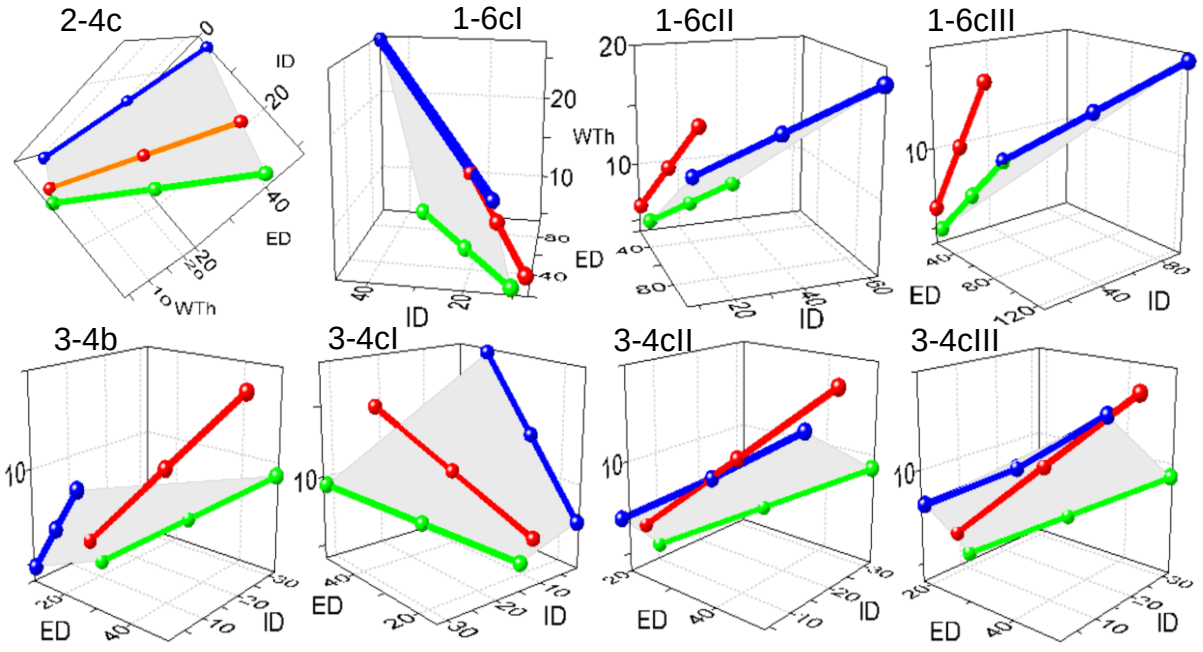
2-4c
1-6cI
1-6cII
1-6cIII
3-4b
3-4cI
3-4cII
3-4cIII
ID
ED
WTh

Fig 20.

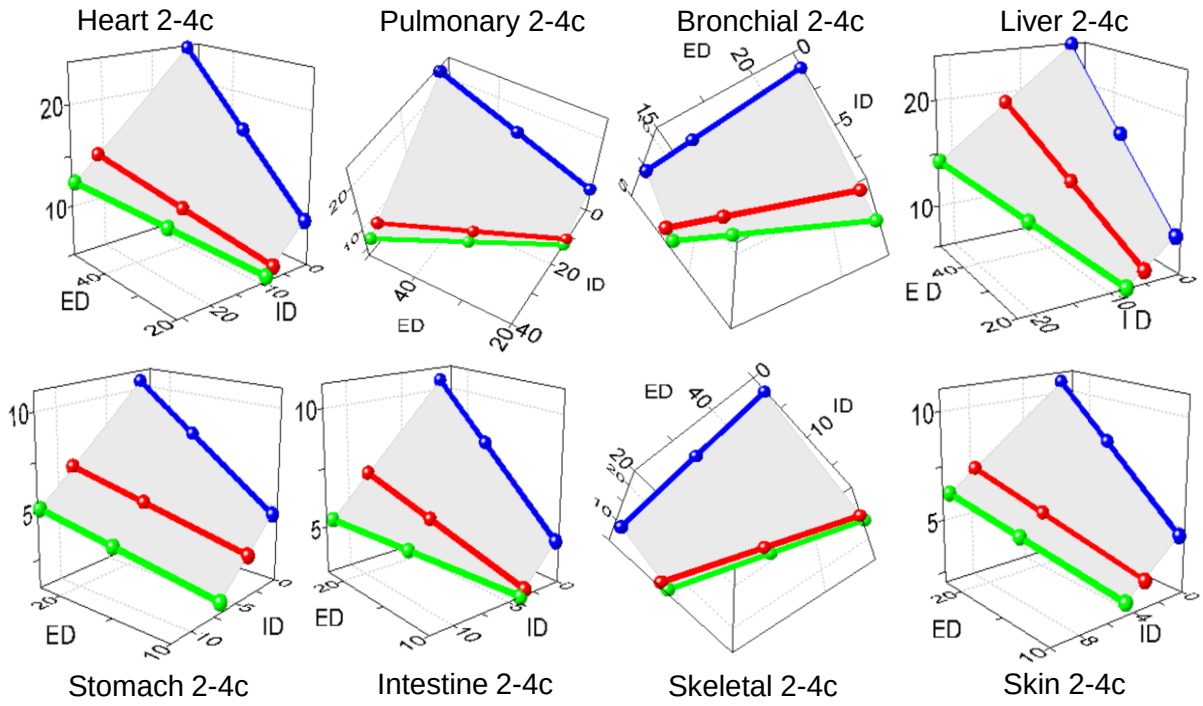
Heart 2-4c
Pulmonary 2-4c
Bronchial 2-4c
Liver 2-4c
Stomach 2-4c
Intestine 2-4c
Skeletal 2-4c
Skin 2-4c
ED
ID

Fig 21.

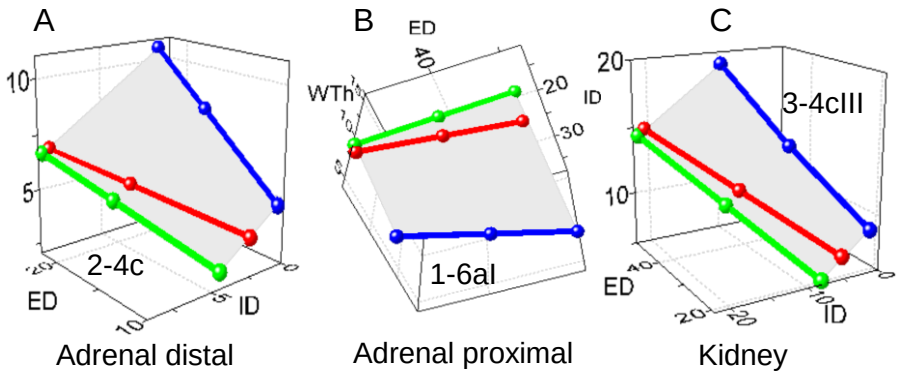
A
B
C
2-4c
1-6aI
3-4cIII
ED
ID
WTh
Adrenal distal
Adrenal proximal
Kidney

Fig 22.

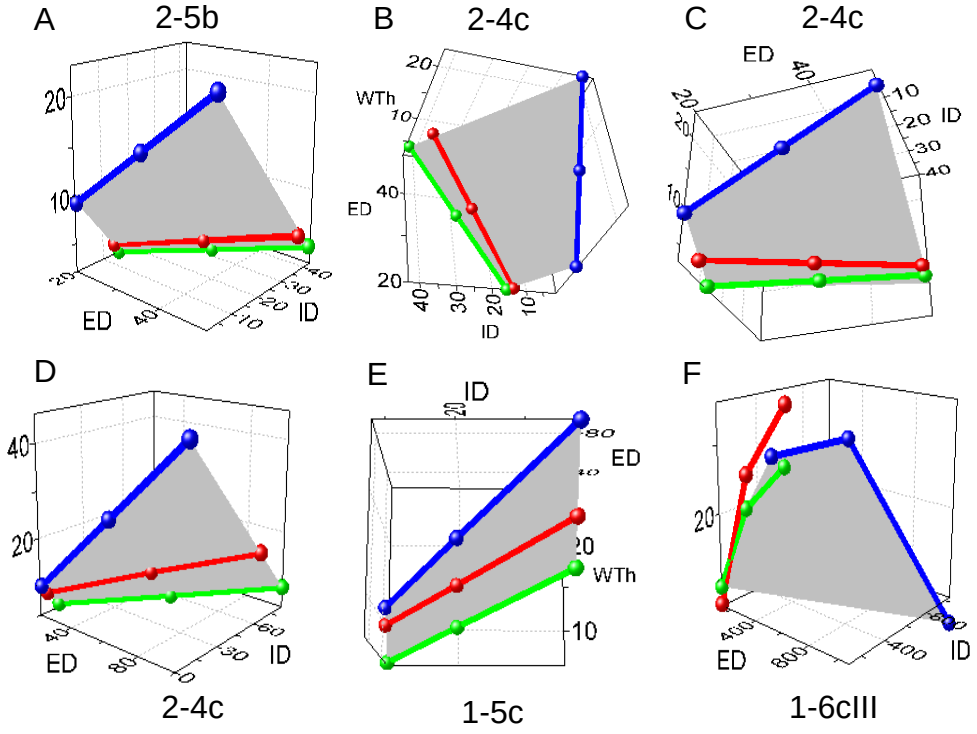
A
2-5b
B
2-4c
C
2-4c
D
E
F
ED
ID
WTh
2-4c
1-5c
1-6cIII

Fig 23.

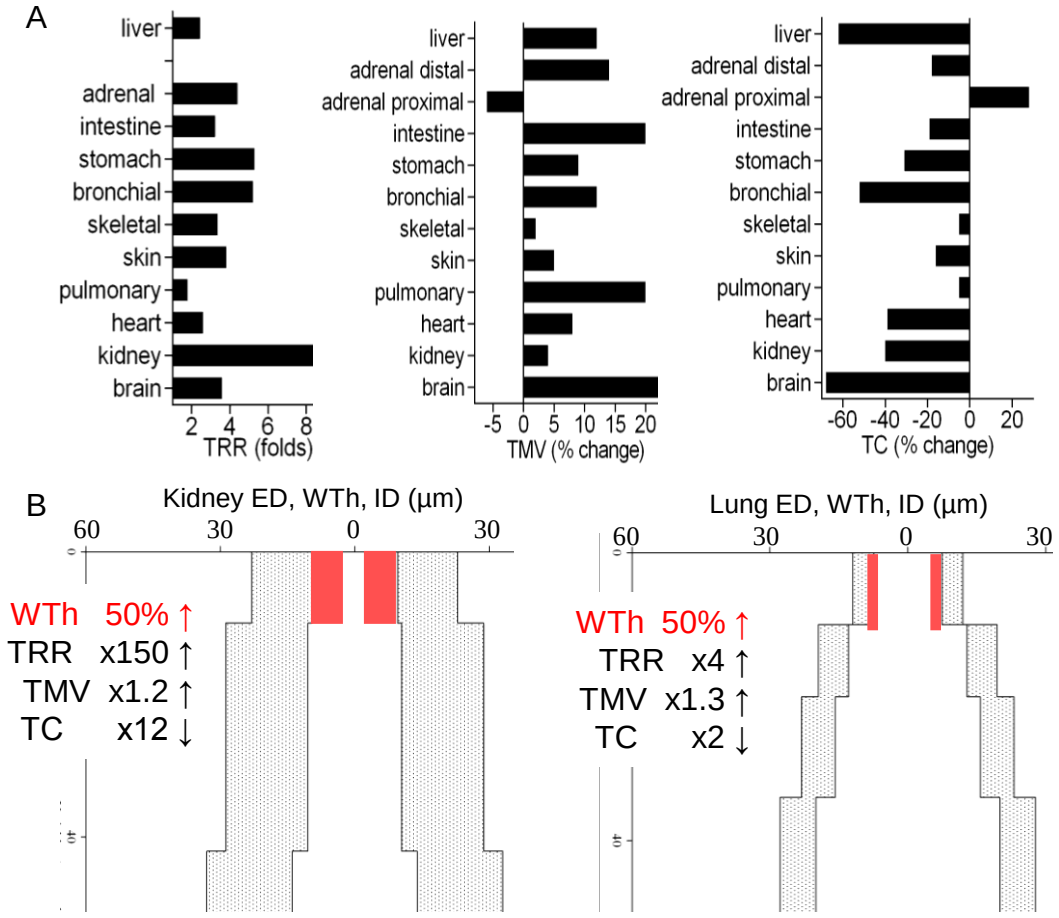
A
liver
adrenal
intestine
stomach
bronchial
skeletal
skin
pulmonary
heart
kidney
brain
2 4 6 8
TRR (folds)
adrenal distal
adrenal proximal
-5 0 5 10 15 20
TMV (% change)
-60 -40 -20 0 20
TC (% change)
B
Kidney ED, WTh, ID (µm)
60 30 0 30
WTh 50% ↑
TRR x150 ↑
TMV x1.2 ↑
TC x12 ↓
Lung ED, WTh, ID (µm)
WTh 50% ↑
TRR x4 ↑
TMV x1.3 ↑
TC x2 ↓

Fig 24.